Springback: improvement of its predictability

Literature study report

I.Burchitz

March 2005
NIMR project MC1.02121

Netherlands Institute for Metals Research

Summary

The deep drawing process is commonly used to manufacture sheet metal products. During the process initially curved or flat blank material is clamped between the die and the blankholder. When the punch is pushed into the die cavity, the blank is plastically deformed and the specific shape of the punch and the die is transferred to it. After the tools are removed, the elastically-driven change of the product shape, or so-called springback, occurs. This phenomenon results into the deviation of the obtained product shape from the design specification and can be the major cause of assembly problems.

In sheet metal forming the quality of the final product depends on the proper tools' design, choice of the blank material, blankholder force, lubrication and some other process parameters. To manufacture a product with the desired shape and performance an extensive knowledge about the influence of various parameters is needed. In order to establish this knowledge base, experimental try-outs or numerical simulations are used. Finite element simulation of sheet metal forming is a powerful tool, which allows to test any modifications of the deep drawing process parameters, prior to the actual tools manufacturing. Calculations can be made to predict and compensate for springback and the numerical simulations can be repeated as often as necessary until the product with the desired shape is produced.

Currently the numerical analysis is not able to accurately predict the springback of a formed product. There is always a discrepancy between the level of springback obtained in simulations and reality, especially for the products with complicated geometry. The objective of this literature study is to understand the springback phenomenon and to ascertain the reasons of its inaccurate numerical prediction. Development of algorithms for improved numerical prediction of springback after trimming operation is a subject of a separate research [1] and is not dealt with in this study.

One of the reasons for poor springback prediction is that this phenomenon is not accurately represented in finite element formulations. Various assumptions of material behaviour - constant elastic properties during forming, simplified elastic-plastic anisotropy and workhardening - introduce the large modelling error. In addition, the accuracy of the springback prediction is affected significantly by the quality of simulation of the forming operation. Chosen contact algorithms, the method of unloading, the time integration scheme, the element types and the level of discretization can be other reasons for significant deviation of the numerically predicted springback from that observed in real practice. Furthermore, an analyst plays an important role and substantial discrepancy of the springback results may be caused by unexperienced users.

Contents

Introduction

In sheet metal forming, the shape of the blank obtained at the end of the forming step closely conforms to the tools' geometry. However, as soon as the loads are removed, elastically-driven change in the blank shape takes place. This process is termed springback. In the automotive industry, engineering guidelines and finite element software are used in the design process for new sheet metal parts. Very often during the design process the level of springback is numerically predicted. Based on this prediction, the tools' geometry and process parameters are modified to obtain the required product shape (figure 1).

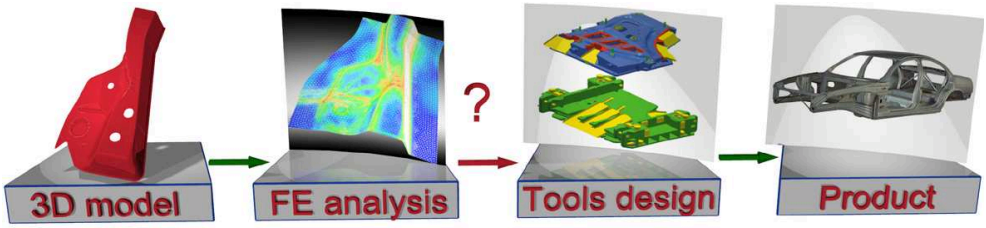

Figure 1: Schematic of the design process.

Unfortunately, the current accuracy of springback prediction is not sufficient [2, 3, 4, 5]. Therefore, there is a need to start an extensive experimental trial and error process to determine the necessary tools' geometry and other variables, which will enable production of the required product shape. As a result, the product cost and the time from design to production are increased considerably.

An accurate prediction and control of springback phenomenon during full process modelling will allow tool designers to numerically evaluate the probability of obtaining the specified product shape and to perform the necessary modifications based on this information only. If the experimental trial and error process is replaced by a reliable numerical procedure, the production time and costs can be decreased drastically. Improving the numerical predictability of springback requires a complete understanding of this phenomenon.

Chapter 1

Analytical methods for springback in forming

Simple analytical solutions for springback in plane-strain pure bending and plane-strain pure bending with superimposed tension were derived several decades ago. These solutions usually assume elastic-perfectly plastic material behaviour [6]. In sheet metal forming, analytical solutions for springback were firstly derived for simple cases, such as: flanging [7,8,9], V-bending [10, 11] and U-bending. The methods were extended to more complicated and realistic cases, such as draw bending [12,13] and stretch bending [14,15,16,17,18], in which tension was accounted for. Special attention was given to the accurate analytical prediction of sidewall curl caused by bending and unbending deformation at the die shoulder.

The authors in [12] presented an analysis tool to predict springback and sidewall curl for plane strain stretch-draw forming (NUMISHEET'93 benchmark problem). Major attention was given to analytical calculation of through-thickness strains and stresses for bending plus stretching and unbending plus stretching situations. The complete method is based on superposition of stretching strains, obtained from the finite-element analysis, and calculated analytically thickness strains. The developed theory was capable of predicting practically observed differences in springback and sidewall curl for different materials. It was reported that slight underestimation of springback was due to employed kinematic hardening law and inability to accurately calculate the restraining force in the blankholder region.

A distinctive study was performed by Zhang and Hu [13]. In this work authors investigated the reasons of great differences found in springback prediction among various researchers. The plane strain stretch bending process together with repeating bending and unbending were studied. The following points were stressed as important:

- deformation history must be tracked for an accurate calculation of stress distribution in the material when it undergoes repeated bending/unbending conditions;
- springback may involve plastic deformation and the natural unloading method can provide more accurate prediction of residual stress distribution, especially for stretch bending.

A detailed analytical description of plane-strain pure bending of a sheet material and pure bending with tension is given in the following section.

1.1 Plane strain draw bending

In this section the mechanics of simple bending, unbending and bending in combination with tension of a sheet is considered. The analytical models are presented, which can be used to predict tensile forces, bending moments and springback.

1.1.1 Strains in bending and stretching

The parameters of the straight line bending problem are shown in figure 1.1. In the analysis the following assumptions are used [19]:

- normal section planes remain plane and normal to the middle surface (Kirchhoff hypothesis);
- plane strain condition exists in the plane perpendicular to the bending line;
- plane stress situation is assumed;
- bends with constant curvature are considered. Within the bends the radial ρ and circumferential directions θ can be distinguished. Due to the Kirchhoff hypothesis the radial and circumferential directions are principal strain directions.

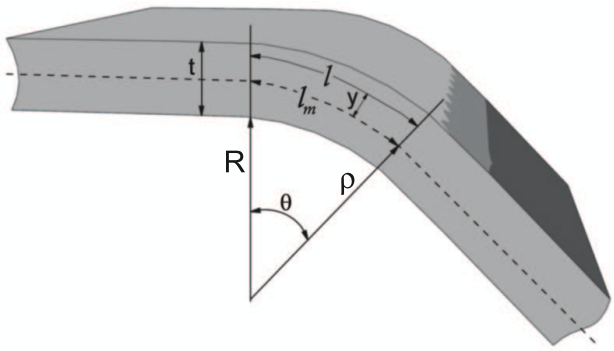

Figure 1.1: Geometrical parameters of pure bending problem.

Bending a strip to an angle θ with a radius of curvature ρ is considered (see figure 1.1). After bending the length of the segment in the mid-surface is $l_m = \rho\theta$. This mid-surface is not necessarily the neutral surface. The neutral surface will shift towards the curvature centre if a tensile force is present or if a small bending radius $R < 3t$ is used. A line segment with initial length l_0 at a distance y above the mid-surface will have a length l after bending. This length can be expressed as follows:

$$l = (\rho + y) \cdot \theta = (1 + \frac{y}{\rho}) \cdot \rho\theta = l_m \cdot (1 + \frac{y}{\rho}) \tag{1.1}$$

Thus, the circumferential strain:

$$\varepsilon_\theta = \ln\left(\frac{l}{l_0}\right) = \ln\left(\frac{l_m}{l_0} \cdot (1 + \frac{y}{\rho})\right) = \ln\left(\frac{l_m}{l_0}\right) + \ln\left(1 + \frac{y}{\rho}\right) = \varepsilon_m + \varepsilon_b \tag{1.2}$$

Where ε_m is the strain in the mid plane and ε_b is the bending strain.

1.1.2 Bending stresses

The Hill'48 criterion is used to describe yielding of the material. In general form it can be written as follows:

$$f = F(\sigma_y - \sigma_z)^2 + G(\sigma_z - \sigma_x)^2 + H(\sigma_x - \sigma_y)^2 + 2L\tau_{yz} + 2M\tau_{zx} + 2N\tau_{xy} - 2\sigma_f^2 = 0 \tag{1.3}$$

F, G, H, L, M and N are the anisotropy parameters of the material, which are determined from the uniaxial tensile and simple shear tests. σ_f is the flow stress.

The Hill'48 yield criterion can be simplified for plane stress situation, since $\sigma_{yz} = \sigma_{zx} = \sigma_z = 0$. Therefore, the equation 1.3 takes the form:

$$f = F\sigma_y^2 + G\sigma_x^2 + H(\sigma_x - \sigma_y)^2 + 2N\tau_{xy} - 2\sigma_f^2 = 0 \Rightarrow \tag{1.4}$$

$$f = (G + H)\sigma_x^2 + (F + H)\sigma_y^2 - 2H\sigma_x\sigma_y + 2N\tau_{xy}^2 - 2\sigma_f^2 = 0$$

If the material is assumed to be planar isotropic its response is independent of the loading direction in the plane. Thus, $R_0 = R_{45} = R_{90} = R \Rightarrow F = G$ and the yield function can be written in terms of the principal stresses. The Hill'48 yield function for plane stress can be simplified even further, since shear stress will disappear from equation 1.4 for formulation in principal directions.

$$(G + H)\sigma_1^2 + (G + H)\sigma_2^2 - 2H\sigma_1\sigma_2 = \sigma_f^2$$

$$\sigma_1^2 + \sigma_2^2 - \frac{2H}{G + H}\sigma_1\sigma_2 = \frac{2\sigma_f^2}{G + H} = \sigma_{un}^2 \tag{1.5}$$

Where σ_{un} is the in-plane uniaxial yield stress. Equation 1.5 can be rewritten in the following way:

$$\sigma_1^2 + \sigma_2^2 - \frac{2H}{(1 + H/G)G}\sigma_1\sigma_2 = \sigma_{un}^2$$

$$\Rightarrow \sigma_1^2 + \sigma_2^2 - \frac{2R}{(1+R)}\sigma_1\sigma_2 = \sigma_{un}^2 \tag{1.6}$$

Based on the Hill'48 yield function the plane strain yield stress can be determined. The plane strain yield stress is characterised by the point on the yield locus with a vertical tangent. In this case:

$$\frac{d\varepsilon_1}{d\varepsilon_2} = -\frac{\frac{\partial f}{\partial \sigma_1}}{\frac{\partial f}{\sigma_2}} \to \infty$$

$$\Rightarrow \frac{\partial f}{\partial \sigma_2} = 2\sigma_2 - \frac{2R}{R+1}\sigma_1 \to 0 \tag{1.7}$$

Now, substitution $\sigma_2 = \frac{R}{R+1}\sigma_1$ and $\sigma_1 = \sigma_{ps}$ into equation 1.6 will yield:

$$\left(\frac{\sigma_{ps}}{\sigma_{un}}\right)^2 = \frac{(R+1)^2}{1+2R} \tag{1.8}$$

Finally, the circumferential stress σ_θ in plane strain bending for isotropic material (R=1) can be defined from equation 1.8 as follows:

$$\left(\frac{\sigma_\theta}{\sigma_{un}}\right)^2 = \frac{4}{3} \Rightarrow \sigma_\theta = \frac{2}{\sqrt{3}}\sigma_{un} \tag{1.9}$$

In the following analysis Nadai hardening will be used. Usually the parameters of Nadai hardening are derived from one dimensional tensile experiments and it is presented as the uniaxial stress σ_{un} as a function of the uniaxial strain ε_{un}. It was already shown that in numerical description of the yield function the equivalent stress σ_f, which is equal to uniaxial stress σ_{un}, is used. It is assumed that the equivalent stress σ_f varies in the same way depending on the uniaxial strain ε_{un}:

$$\sigma_f = C\varepsilon_{un}^n \tag{1.10}$$

To be applicable to the current analysis the hardening relation needs to be extended to two dimensional case. It is known that for many metals the hardening is the function of the plastic work done per unit volume in case of proportional loading. If the ratio between the components of the stress and strain tensors remain constant ($\alpha = \sigma_2/\sigma_1$, $\beta = \varepsilon_2/\varepsilon_1$) the loading is proportional. Based on this consideration the relation, which can describe the expression of any component of the stress tensor as a function of any component of strain tensor can be derived:

$$\sigma_{ij} = C'\varepsilon_{ij}^n \tag{1.11}$$

Taking into account equation 1.9 the circumferential strain for proportional loading can be defined as follows:

$$\sigma_f d\varepsilon_{un} = \sigma_\theta d\varepsilon_\theta \;\Rightarrow\; \sigma_f d\varepsilon_{un} = \frac{2}{\sqrt{3}}\sigma_f d\varepsilon_\theta$$

$$\Rightarrow\; \varepsilon_\theta = \frac{\sqrt{3}}{2}\varepsilon_{un} \tag{1.12}$$

The relation between circumferential stress and strain in case of proportional loading and plane strain situation can be found based on the plastic work expression:

$$\frac{W}{\Delta V} = \int_0^{\varepsilon_\theta} \sigma_\theta d\varepsilon_\theta = \int_0^k \sigma_f dk \;\Rightarrow\; \int_0^{\varepsilon_\theta} C'\varepsilon_\theta^n d\varepsilon_\theta = \int_0^k Ck^n dk$$

$$\Rightarrow\; C'\varepsilon_\theta^{n+1} = Ck^{n+1} \;\Rightarrow\; C' = C\Big(\frac{k}{\varepsilon_\theta}\Big)^{n+1}$$

Using equation 1.12 the value C' becomes:

$$C' = C\Big(\frac{2}{\sqrt{3}}\Big)^{n+1} \tag{1.13}$$

Based on the value of circumferential stress, the forces and bending moments acting on the sheet per unit length are found from:

$$T = 2\int_0^{t/2} \sigma_\theta dy \tag{1.14}$$

$$M = 2\int_0^{t/2} \sigma_\theta y dy \tag{1.15}$$

1.1.3 Simple bending

Loading. For simple bending problem the tension is not present and therefore the equation for the circumferential strain 1.2 can be simplified:

$$\varepsilon_\theta = \ln\Big(1 + \frac{y}{\rho}\Big)$$

If the bending radius is much larger than the sheet thickness the circumferential strain can be simplified even further:

$$\varepsilon_\theta = \frac{y}{\rho} \tag{1.16}$$

The circumferential stress in any point of the cross-section can be found by:

$$\sigma_\theta = C'\Big(\frac{y}{\rho}\Big)^n \tag{1.17}$$

The total bending moment is found by means of equation 1.15:

$$M = 2\int_0^{t/2} \sigma_\theta y dy = 2\int_0^{t/2} C'\Big(\frac{y}{\rho}\Big)^n y dy = 2C'\frac{t^{n+2}}{\rho^n(n+2)2^{n+2}}$$

$$\Rightarrow \quad M = \frac{C't^2}{2(n+2)}\Big(\frac{t}{2\rho}\Big)^n = \frac{\sigma_\theta t^2}{2(n+2)}\Big(\frac{t}{2y}\Big)^n \tag{1.18}$$

In the elastic region, when $n = 1$ and Hooks law applies ($C' = E/(1-\nu^2)$), the bending moment is defined by the following equation:

$$M = \frac{Et^2}{6(1-\nu^2)}\frac{t}{2\rho} = \frac{\sigma_\theta t^3}{12y} \tag{1.19}$$

From the foregoing equation 1.19 the expression for the corresponding elastic curvature can be found:

$$\frac{1}{\rho_e} = \frac{\sigma_\theta(1-\nu^2)}{Ey} \tag{1.20}$$

If the circumferential stress σ_θ at the surface of the sheet $y = t/2$ becomes equal to the plane strain yield stress $S_0 = (2/\sqrt{3})\sigma_f$ the elastic limit is reached. The elastic limit bending moment can be found as follows:

$$M_e = \frac{\sigma_\theta(t^2)}{2(1+2)}\Big(\frac{t}{2t/2}\Big) = \frac{S_0 t^2}{6} \tag{1.21}$$

Corresponding elastic limit curvature:

$$\frac{1}{\rho_e} = \frac{2S_0(1-\nu^2)}{Et} \tag{1.22}$$

In case of rigid, perfectly plastic deformation, when $n = 0$ and $\sigma_\theta = S_0$ (constant yield stress), the bending moment becomes:

$$M_p = \frac{S_0 t^2}{4} \tag{1.23}$$

Unloading. It is clear that the external bending moment applied by the tools and the internal moment resisting bending must be equal. When the tools are removed, the external moment becomes zero and therefore the internal moment must also vanish. During springback the material unbends elastically and the magnitude of internal stresses will decrease. The final stress distribution results in zero bending moment. The change of internal stresses due to elastic unloading:

$$\Delta\sigma_\theta = \frac{E}{1-\nu^2}\Delta\varepsilon_\theta, \tag{1.24}$$

$$\Delta\varepsilon_\theta = \frac{y}{\rho} - \frac{y}{\rho'}$$

where ρ' is the value of the bending radius after unloading. The change in internal stresses causes the change in bending moment, ΔM:

$$\Delta M = 2\int_0^{t/2} \Delta\sigma_\theta y dy = 2\int_0^{t/2} \frac{E}{1-\nu^2}\Delta\Big(\frac{1}{\rho}\Big)y^2 dy$$

$$\Delta M = \frac{Et^3}{12(1-\nu^2)}\Delta\Big(\frac{1}{\rho}\Big) = \frac{t^3}{12}\frac{\Delta\sigma_\theta}{y} \tag{1.25}$$

If the bending moment is $M = St^2/4$ the release of tools results in $\Delta M = -St^2/4$. Therefore the change of shape during unloading can be obtained:

$$\frac{Et^3}{12(1-\nu^2)}\Delta(\frac{1}{\rho}) = -\frac{S_0 t^2}{4}$$

$$\Delta\frac{1}{\rho} = -\frac{3S_0(1-\nu^2)}{Et} \tag{1.26}$$

Based on equation 1.26 the change of bending angle $\Delta\theta$ can be derived. Due to the fact that the arc length l of the bend remains constant during bending and springback one can write:

$$l = \rho\theta = \frac{\theta}{1/\rho} = \frac{\theta + \Delta\theta}{1/\rho + \Delta 1/\rho}$$

After substituting the value of $\Delta 1/\rho$ into the foregoing equation and solving it for $\Delta\theta$:

$$\Delta\theta = -\theta\frac{\rho}{t}\frac{3S_0(1-\nu^2)}{E} \tag{1.27}$$

From equation 1.27 the following conclusions can be drawn for situation when bending is present:

- elastic springback is higher for smaller values of Young's modulus;
- elastic springback is higher for higher values of the yield stress;
- elastic springback decreases if the relative bending radius decreases.

1.1.4 Bending with tension

Stretching the sheet that is already bent. For simplicity, elastic perfectly plastic material model is considered. At first the sheet is bent elastically, which means that the bending radius is larger than the limiting ρ_e (see equation 1.22). In this elastic situation the bending moment M can be identified from equation 1.19. The ratio between the current M and the limiting M_e bending moments can be defined as follows:

$$\frac{M}{M_e} = \frac{\rho_e}{\rho} \tag{1.28}$$

If the tension is applied after applying bending loads the circumferential stress, defined in equation 1.19, will be a superimposition of bending and tensile stresses:

$$\sigma_\theta = \sigma_b + \sigma_t = \frac{12My}{t^3} \tag{1.29}$$

Thus, the tension stress needed to cause plastic deformations in the outer layers of the sheet is defined as follows:

$$\sigma_t = \sigma_\theta - \frac{12My}{t^3} = S_0 - \frac{12My}{t^3} \tag{1.30}$$

Therefore the tension needed to cause plastic deformation in the outer layers of the sheet:

$$T = S_0 t - \frac{6M}{t} = T_y\Big(1 - \frac{6M}{S_0 t^2}\Big) = T_y\Big(1 - \frac{\rho_e}{\rho}\Big) \tag{1.31}$$

This tensile force causes the plastic deformation in the outer fibres of the sheet. Increase of the tension will result into a plastic zone, which will grow towards the sheet centre. If η is the elastic portion of the sheet thickness the tension and the bending moment can be written as follows [19]:

$$T = T_y\Big(1 - \eta^2\frac{\rho_e}{\rho}\Big) \tag{1.32}$$

$$M = M_e\eta^2(3 - 2\eta) \tag{1.33}$$

From the foregoing expressions, for given assumptions, it can be seen that with decreasing η the tension increases, and the bending moment decreases rapidly. Thus, if due to tools geometry or process conditions the sheet is fully plastic, no elastic springback will take place.

Bending the sheet that is already under tension. Figure 1.2(a) presents the draw bending process. The sheet material is drawn over a tool radius and bending is applied after tension. During the process the material, when it passes the tool radius is bent and subsequently straightened or unbent. The distribution of the circumferential strain through the thickness

will comprise of two parts, the tensile strain ε_m and the bending strain ε_b (see equation 1.2). The tensile strain ε_m is constant across the section.

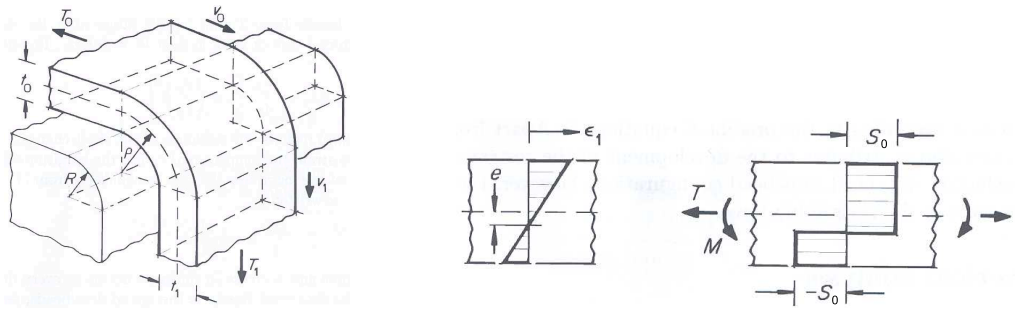

(a) general scheme (b) strains and stresses through the thickness

Figure 1.2: Bending and unbending over a tool radius under the influence of drawing tension T_1 and back tension T_0. Stress and strain distributions through the thickness.

If e is the shift of the neutral line from the mid plane, then:

$$\varepsilon_m = \frac{e}{\rho} \tag{1.34}$$

Assuming that the bending strain $\varepsilon_b = y/\rho$ the total strain through the thickness becomes:

$$\varepsilon_\theta = \frac{(e+y)}{\rho} \tag{1.35}$$

For simplicity rigid, perfectly plastic material behaviour is considered. The stress and strain distribution through the thickness are shown in figure 1.2(b). When the material enters the bending zone the resulting tension is:

$$T_0 = S_0(t_0/2 + e) - S_0(t_0/2 - e) = 2Se \tag{1.36}$$

The shift of the neutral line can be found by substituting into the previous equation value of yield stress $S_0 = T_y/t$:

$$e = \frac{1}{2} t_0 \frac{T_0}{T_y} \tag{1.37}$$

The total plastic work done per unit loading can be described by [19]:

$$dW = \frac{S_0}{2\rho}\Big((t_0/2 + e)^2 + (t_0/2 - e)^2\Big)dl \tag{1.38}$$

Using equation 1.37 the rate of plastic work for bending region can be written as:

$$\dot{W} = \frac{S_0 v_0 t_0^2}{4\rho}\left(1 + \left(\frac{T_0}{T_y}\right)^2\right) \tag{1.39}$$

Where v_0 is the velocity of the material entering the bending region. This amount of plastic work is done by tension T_1 after the bending/unbending region. The net external rate of plastic work will then be $\dot{W} = (T_1 - T_0)v_0 = \Delta T v_0$. From this equation the change of tension due to bending/unbending region can be calculated:

$$\Delta T_0 = \frac{T_y t_0}{4\rho}\left(1 + \left(\frac{T_0}{T_y}\right)^2\right) \tag{1.40}$$

In the considered plane strain situation the thickness strain ε_t equals the tensile strain ε_m. Substituting the shift of the neutral line (equation 1.37) into equation 1.34 the thickness strain can be obtained:

$$\varepsilon_t = -\frac{e}{\rho} = -\frac{1}{2}\frac{t_0 T_0}{\rho T_y} \tag{1.41}$$

Every time, when sheet material undergoes bending and unbending a decrease in sheet thickness and an increase in tension takes place. The application of drawbeads, used to control the material flow during deep drawing, is based on this fact. Several regions of bending and unbending can be distinguished for a sheet passing a drawbead. In every deformation region the sheet thickness decreases and tensile force increases. Apart from the plastic deformation, friction also contributes to the development of the drawbead restraining force [19]. The drawbead is a self-adjusting tool which increases the restraining force when stronger sheet material is used.

In spite of the amount of knowledge developed in the field of analytical prediction of springback most of the methods have little relevance to realistic industrial forming operations in which complicated deformation paths are present [20]. The underlying assumptions of these methods, simplified contact and friction conditions are the major reasons which make them inapplicable for industrial use [21].

1.2 Springback as physical and numerical phenomenon

To be able to efficiently use a finite element software to predict springback in sheet metal forming, springback needs to be considered as a complex physical phenomenon, which is very sensitive to numerous factors (see figure 1.3). It is always difficult to establish the cause of discrepancy between the magnitudes of springback obtained in simulation and reality, especially when the product geometry is complicated [22]. Springback phenomenon in metals depends on various parameters: variation of elastic properties of a material; elastic-plastic anisotropy; material hardening. If finite element modelling is employed for analysis of springback the accuracy of obtained solution is significantly affected by the factors that control the quality of simulation of forming operation. The most important of them include the method of unloading, time integration scheme, choice of element, blank and tool discretization and contact algorithm.

Some of the mentioned factors are relatively simple to take into consideration and their influence on predictability of springback is unambiguous. However, there are factors that

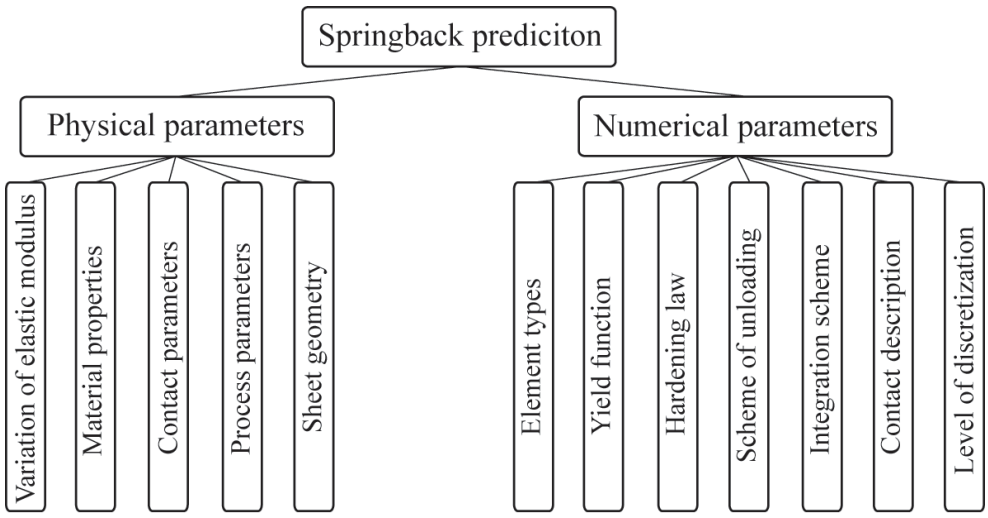

Figure 1.3: Parameters influencing springback prediction.

require careful treatment and extra attention. Material modelling, for example, requires not only a careful selection of an appropriate yield function, but also an extensive analysis of springback characteristics of sheet metal by means of different test procedures [22].

Authors in [23], based on the results of one of the NUMISHEET'02 benchmark problems, investigated the reasons of scatter of results in springback prediction. It was concluded, that amongst various reasons, an analyst plays an important role and substantial discrepancy of springback results may be caused by unexperienced users.

Chapter 2

Understanding springback phenomenon

This chapter provides an overview of experimental procedures used to understand the springback phenomenon in sheet materials. The reasons of decrease of material elastic modulus during the deformation are discussed. The chapter is finished with the description of important features of a material behaviour, which must be taken into consideration during material modelling.

2.1 Experiments to study springback in metals

Various experimental techniques and procedures have been developed to study and characterise springback of sheet metals. The most popular and commonly used techniques are cylindrical bending [23], U-bending [24, 25], V-bending [25, 26, 27] (see figure 2.1) and flanging [7, 9]. These methods are attractive because the level of springback is large and it

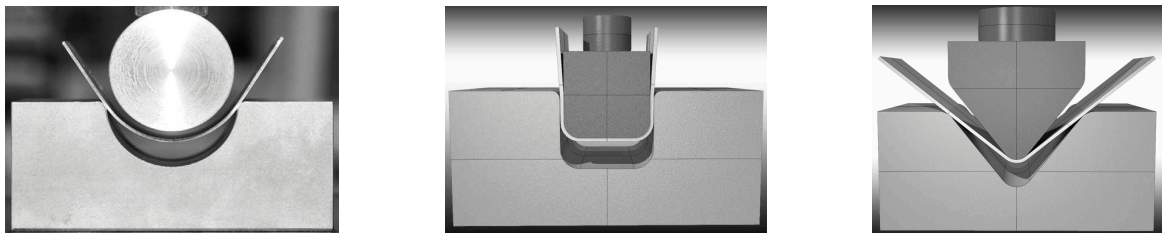

(a) cylindrical bending (b) U-bending (c) V-bending

Figure 2.1: Most commonly used experimental techniques for studying the springback of metals.

can easily be measured. Sensitivity of springback to basic parameters, such as R/t ratio (tool radius to sheet thickness), geometric parameters of the tools, mechanical properties of sheet material and friction parameters is usually studied by means of these techniques. The major drawback of these experiments is that they cannot imitate the realistic process conditions that take place during sheet metal forming [21].

Stretch bending tests are used to study the importance of tension in minimising and controlling springback [22] (see figure 2.2). The application of these experimental procedures for studying the bending/unbending situation and large sliding over the tools' surface is arguable. In spite of the fact that the material undergoes bending and unbending under tension at the drawbead region (as shown in figure 2.2), the careful control of experimental parameters to study this common phenomenon of forming operations is problematic. The top-hat section test (see figure 2.3(a)), presented as a benchmark problem at

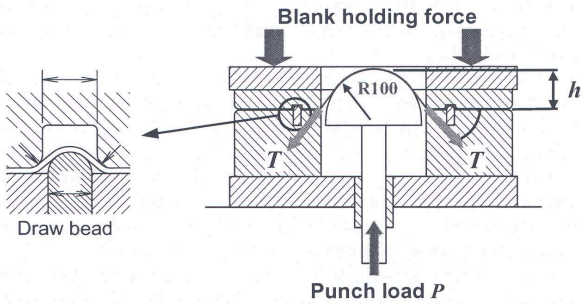

Figure 2.2: Schematic of stretch bending test.

the NUMISHEET 1993 conference, is often used to assess springback in sheet metals under realistic forming conditions. During forming, the blank material experiences stretching, bending and unbending deformations when it passes the tool radius. This deformation path creates complex stress-strain states resulting in the formation of so-called sidewall curl (see figure 2.3(b)). Various authors have used this experimental set-up to study springback and sidewall curl in particular [12, 28, 29, 30]. It has been shown that the sidewall curl becomes more pronounced for small tool radii and smaller clearances between the tools [12]. The

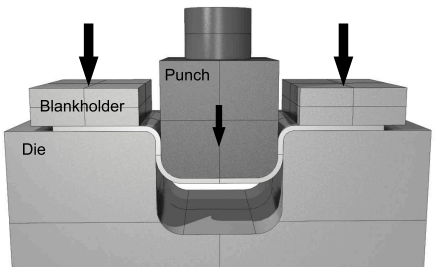

(a) set-up schematic

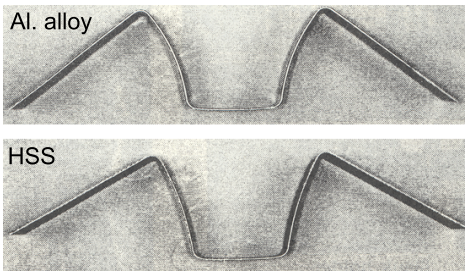

(b) springback and sidewall curl

Figure 2.3: Top-hat section test. NUMISHEET 1993 benchmark.

major drawback of the top-hat section test is the lack of control or direct measurement of sheet tension, which makes this experimental procedure less suitable for verifying the results of simulations [6, 21, 2, 31]. In this test the sheet tension can only be determined indirectly, for example, from the binder force and the coefficient of friction, usually known only approximately. Carden et al. in [6] suggested an alternative experimental procedure to be used to study springback in sheet metals and its sensitivity to various parameters. The general schematic of the draw/bend test is shown in figure 2.4. The experimental

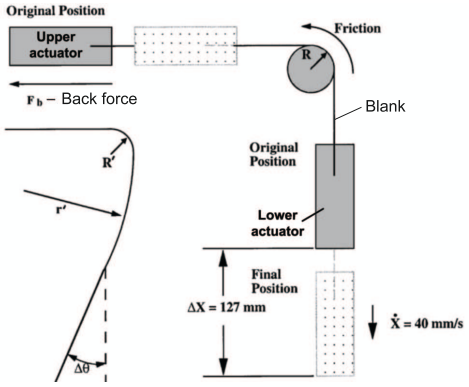

Figure 2.4: General scheme of the draw/bend test.

set-up consists of upper and lower actuators oriented 90° to one another. Placed at the intersection of their action lines there is a cylinder, which represents the tooling radius. The upper actuator provides a constant restraining force, while the lower actuator is used to displace the blank at a constant speed. When drawn over the tool radius, the blank undergoes tensile loading, bending and unbending [6]. The test is considered as a well-characterised example of a forming operation that emulates real process conditions and has the advantage of simplicity [21].

It is known that the isotropic or kinematic workhardening material models are not able to produce an accurate stress state after combined stretching, bending and unbending deformation. The importance of taking into account the deformation history has been stressed by various authors [12, 13]. Several experimental procedures were developed to study the sensitivity of springback to the Bauschinger effect. The uniaxial tension-compression or compression-tension test is the most common experimental procedure [32, 33]. A simple method was presented in [34] (see figure 2.5). After prestraining the sheet sample to 6% in uniaxial tension, its uniform part is cut into 10 small segments (figure 2.5(a)), which are then bonded together with the original tensile axes aligned. After that the newly obtained sample is tested in compression and the compressive loading continues until about 1% of plastic strain is obtained (figure 2.5(b)).

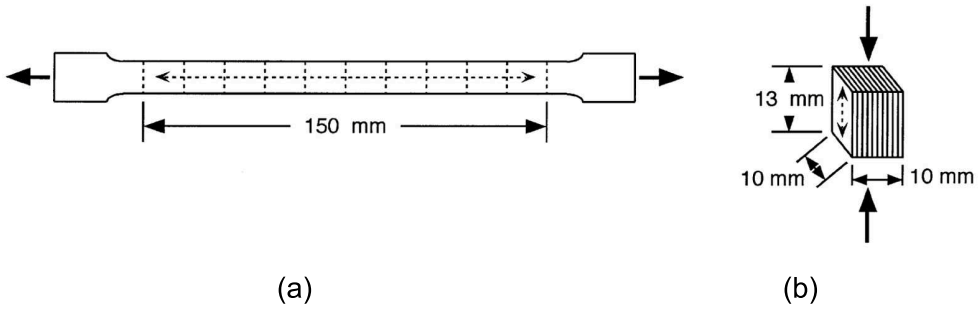

Figure 2.5: Schematic of the method used for tensile prestraining followed by compression.

Cyclic uniaxial compression-tension tests require special fixtures to be used to prevent the sheet material from buckling under compression. Yoshida et al. [35] presented the experimental set-up, which can be used to study the elastic-plastic stress-strain responses of sheet material under in-plane cyclic tension-compression under large strain. The schematic of the set-up is illustrated in figure 2.6(a). To prevent buckling under compression, several pieces of the sheets were bonded together. In addition, an anti-buckling device was attached to the specimen by coil-springs (see figure 2.6(b)). Friction between the device and the sheet specimen was reduced by employing lubrication. It was observed that with the anti-buckling device it was possible to apply large strain reversals of about 10%.

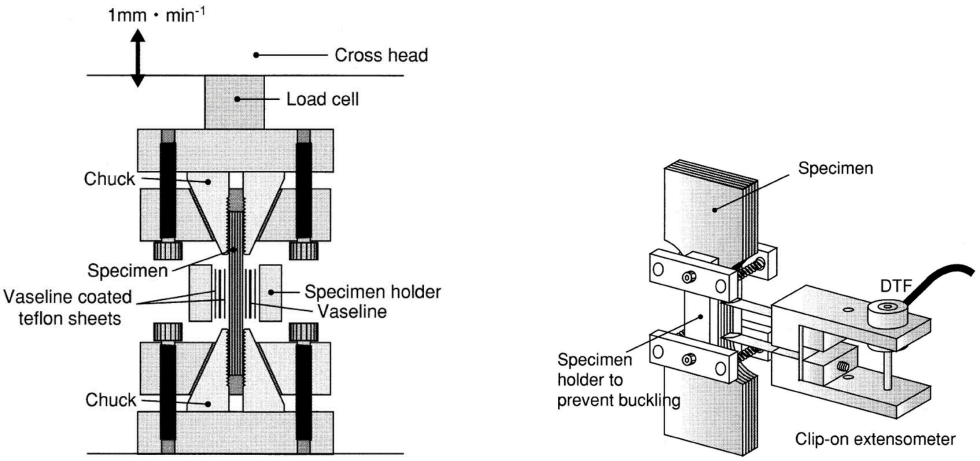

(a) set-up (b) anti-buckling device

Figure 2.6: Schematic of the in-plane cyclic tension-compression test.

To completely overcome the buckling problem, pure bending and reverse bending tests (as shown in figure 2.7), were developed [32, 36, 37]. It is shown in this figure, that the punch

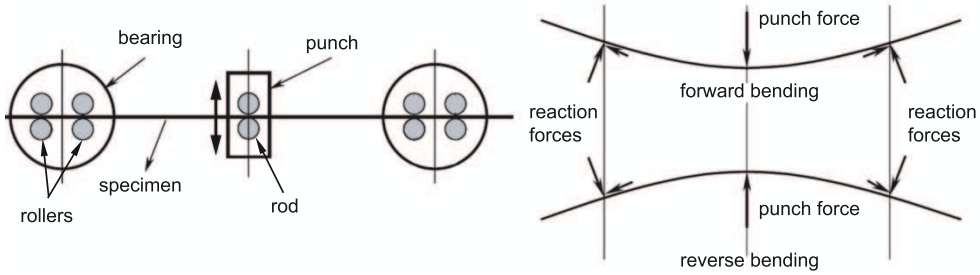

Figure 2.7: Schematic of cyclic three-point bending test.

consists of two aligned, non-rotating rods that clamp the blank to prevent any possible sliding. The lower fixture consists of two freely rotating bearings. Four rotatable rollers are fixed into each bearing. The position of the rods is adjustable to accommodate the material with various thicknesses. During the test, the punch performs vertical movement and the punch force and displacement are recorded. In this test, the relationship between

stress and strain cannot be obtained directly and the Bauschinger effect can be observed only from the load-displacement curve.

A simple bending-reverse bending experimental method was proposed in [38, 39]. As illustrated in figures 2.8, 2.9 the experimental procedure consists of several steps: bending, turning the sheet specimen and bending in the opposite direction, turning the specimen again and bending it in the original direction, and so on. The angle after springback is measured by the coordinate measuring machine and the dependency of this angle on the deformation history can then be easily observed.

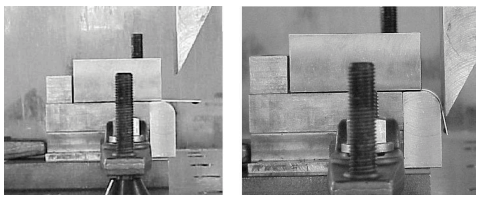

Figure 2.8: Some steps of deformation sequence during bending process.

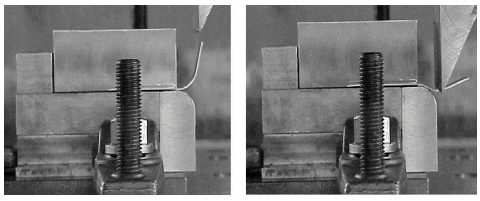

Figure 2.9: Some steps of deformation sequence during reverse bending process.

A shear test can also be used to study the Bauschinger effect in sheet metals [40]. The schematic of the test is shown in figure 2.10. In the process, the clamping parts are moved relative to one another and the zones between them undergo shear deformations. High strains in sheet specimen can be achieved using this method.

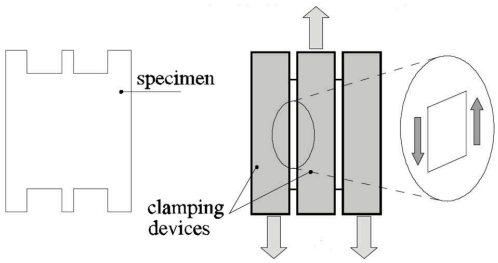

Figure 2.10: Schematic of the shear test.

There is a sufficient experimental literature dealing with understanding and characterising the springback phenomenon of sheet metals. However, the experimental methods - that are capable of imitating bending and unbending with superimposed tension, sliding over the tools' surfaces and that allow careful control of experimental parameters - are less common.

2.2 Variation of elastic properties of metals

Springback depends on Young's modulus of a material. In analysis of sheet metal forming it is a common practice to assume that Young's modulus is constant. However, exper-

imental investigations revealed that elastic constants of a material may change during plastic deformation.

2.2.1 Influence of lattice defects on elastic modulus

The decrease of elastic modulus after a certain amount of cold workhardening was extensively studied by Lems [41]. It is known that lattice defects (point defects and dislocations) in metals influence their elastic behaviour. Even simple presence of point defects, namely interstitials and vacancies, changes the elastic constants of a material as the atomic bonds are disturbed. However, due to the fact that concentrations of points defects are usually very low this effect may be considered negligible.

According to Lems lattice defects may contribute to non-elastic strain by moving under the influence of applied stress. In the presence of lattice defects movements the total strain is the sum of the pure elastic and the non-elastic strain. Thus for a given elastic stress the strain is larger causing the apparent decrease of the elastic modulus. If E_0 is the original elastic modulus of a material and ε is the pure elastic strain, then the magnitude of the decrease may be expressed as follows [41]:

$$\frac{E - E_0}{E_0} = \frac{\Delta E}{E_0} = -\frac{\varepsilon_{non}}{\varepsilon + \varepsilon_{non}} \tag{2.1}$$

Where E is the observed value of the elastic modulus in the presence of lattice defects and their non-elastic contribution to the total strain is represented by ε_{non}.

Diffusion of vacancies and interstitials can make the dimensions of the body to change and therefore may contribute to the non-elastic part of the strain. In a body centred cubic crystal (b.c.c) under the applied stress the interstitial impurities jump to the interstitial sites, which provide more room for them. These local changes contribute to the non-elastic strain. However, this effect will not develop in face centred cubic crystals (f.c.c.). In f.c.c. crystal an interstitial atom or a vacancy that occupies the centre of the cube will not contribute to the elastic strain, since the stress does not provide preferential sites for them. It is known, however, that the contribution of point defects to the non-elastic strain is small since their concentration is small. Movements of point defects cannot cause changes in the elastic modulus greater than about 0.1%.

Under applied stress the small reversible displacement of dislocations takes place, which builds the non-elastic part of the total strain and ultimately causes the decrease of elastic modulus of a material. Several models were developed to describe this effect quantitatively. Some of the models treat the dislocation as an elastic string, which bows out under the influence of applied stress. Yet another model describes the change of elastic constants caused by the change of width of extended dislocations during loading. Other models take into account the atomic structure of the crystal itself and give relatively good prediction of change of elastic modulus. An extensive overview of some models may be found in the original text [41].

Based on experimental observations the following model was proposed in [41] to describe the change of elastic modulus:

$$-\frac{\Delta E}{E} = \frac{24\Lambda L^2}{1 + 24\Lambda L^2} \tag{2.2}$$

Where Λ is the dislocation density and L is the dislocation length.

2.2.2 Experimental investigation of change of elastic constants

The decrease of elastic constants of a material was studied extensively by many of researchers. Lems [41] investigated the decrease of Young's modulus after the tensile deformation at low temperatures, $78°K$. Copper, silver and gold were used as experimental materials. The deformation and measurements were conducted at low temperatures to separate two effects, namely the decrease of elastic modulus and its subsequent recovery. The experimental apparatus is shown in figure 2.11 and briefly described below. It consisted of the

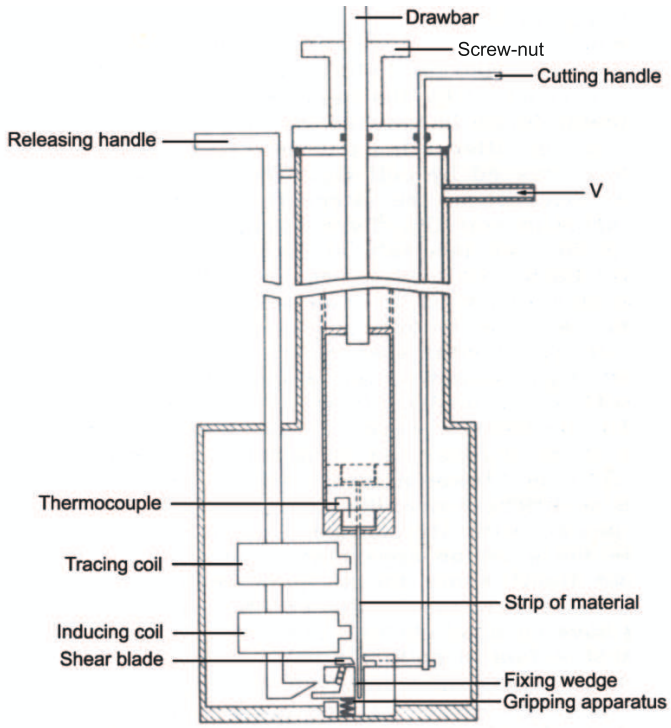

Figure 2.11: Schematic of the experimental apparatus.

major pot, in which the main drawbar is placed. The strip of a material is connected to the drawbar. At the bottom of the pot there is a gripping apparatus, which contains a fixing wedge. To reach an uniaxial plastic deformation state the drawbar is moved down to push the material strip into the gripping apparatus. Afterwards the drawbar is pushed upwards by turning the screw-nut, while the material strip remains fixed in the gripping apparatus by the wedge. After the deformation process the strip is unfixed by turning the releasing

handle, which pushes the fixing wedge down. The shear blade, activated by the cutting handle, is used to cut the material strip to get rid of the region with non-uniform deformation. The temperature of the strip was measured by a thermocouple. The formation of ice on the strip was prevented by evacuating the pot through the opening V. Young's modulus was measured dynamically, by determining the natural frequencies of a strip, using the following relation [41]:

$$E = \frac{48\pi^2 \rho l^4 f^2}{d^2 m^4} \tag{2.3}$$

Where f is the natural frequency of the strip in cycles per second, l is the length of the strip, d is the thickness, ρ is the density and m is a constant, where $m = \frac{\pi}{2}(1.1194; 2.988; 5.0; 7.0; ...)$ for respectively the first, second, ... natural frequencies. An alternating current is sent through an inducing coil, which induces currents in the strip. These currents are attracted or repelled by the permanent magnet in inducing coil, depending on their direction. Therefore a varying force is exerted on the strip with the same frequency as the alternating current of inducing coil. Tracing coil identifies the amplitude of vibrations. By varying the frequency of alternating current the natural frequencies of the strip can be found. The change of Young's modulus is found from equation 2.3 by measuring one of the natural frequencies of the strip before and during the stepwise increase of deformation.

The experimental results for copper and silver are shown in figures 2.12 and 2.13. As can

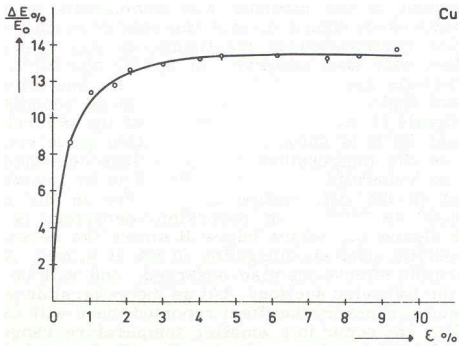

Figure 2.12: Change of Young's modulus of copper (Cu) as a function of deformation at $78°K$.

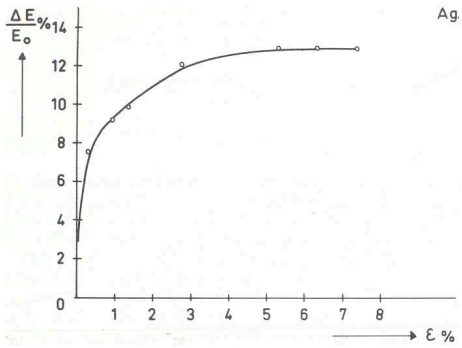

Figure 2.13: Change of Young's modulus of silver (Ag) as a function of deformation at $78°K$.

be seen the saturation value for $\frac{\Delta E}{E}$ of about 14% is reached for both materials.

During the experiments the recovery of the elastic modulus of the materials was observed and studied. Recovery process is taking place during and after the deformation performed at room temperature. The recovery process is shown in figure 2.14 for copper only. This figure clearly shows that elastic modulus increases with time towards its original value.

The fact that workhardening of steels and aluminium alloys can cause an appreciable decrease in Young's modulus was emphasised by various authors [34,42,43,44,45]. Morestin et al. [42] studied the evolution of Young's modulus depending on the plastic strains up to a level of 15%. A tensile-compression test machine was used to conduct the experiments on steel specimen and to investigate the decrease of elastic modulus under pure tension or pure compression. The dependency of the Young's modulus on the plastic strain in case

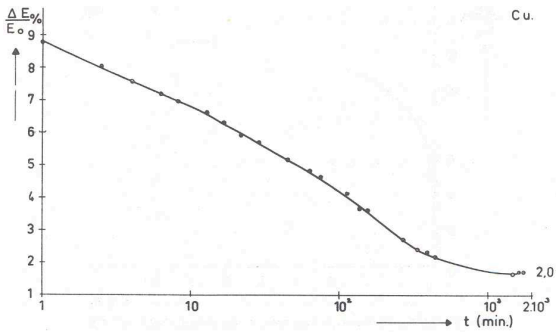

Figure 2.14: Recovery of E modulus of copper as a function of time.

of steel specimen is shown in figures 2.15 and 2.16. It is shown that the diminishing of E modulus can reach a value of 20%.

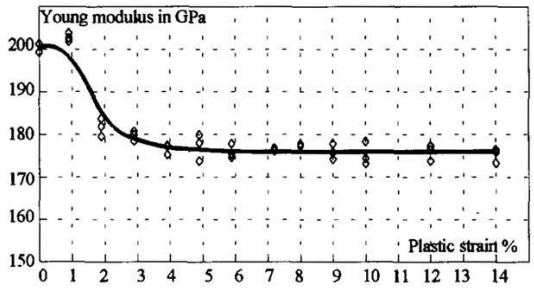

Figure 2.15: Elastic modulus versus plastic strain in pure tension, steel specimen.

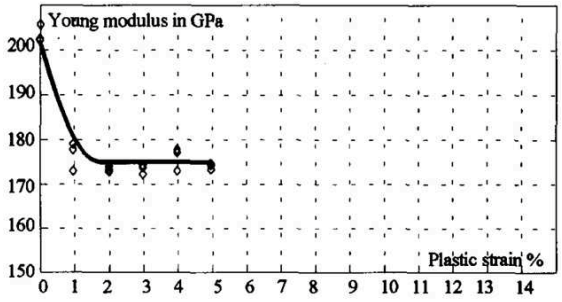

Figure 2.16: Elastic modulus versus plastic strain in pure compression, steel specimen.

In the course of experiments it was also observed that after several weeks the Young's modulus of the deformed specimen recovered its initial value. Figure 2.17 presents the variation of the Young's modulus versus time. Authors explained the phenomenon of recovery by the fact that the dislocations inside the metal move more rapidly than the interstitial carbon atoms that clamp them in the undeformed state. The recovery of Young' modulus can be explained by the slow migration of the carbon atoms towards the new positions of the moved dislocations.

Likewise Lems [41], Thibaud et al. [44] used a vibration method to determine the evolution of E modulus of steel specimen. The authors argued the application of tensile test for determination of Young's modulus, since for some materials the linear part of the stress strain curve is difficult to observe. At the same time the ultra-sound method is not applicable for sheet materials if the measurement directions are important. The Young's modulus of steel specimen was found from the analytical expression of the first natural frequency, which is based on Kirchhoff plate vibration theory. Figure 2.18 summarises the method used and figure 2.19 shows the determined evolution of the elastic modulus.

An interesting study was reported by Yang et al. [45]. Authors employed a precision extensometer and the elastic modulus of aluminium alloy was measured from the stress-strain

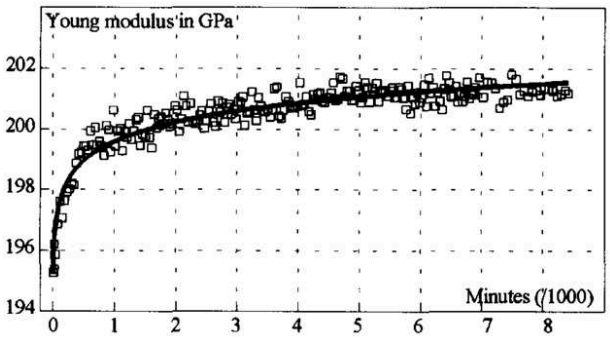

Figure 2.17: E modulus of steel specimen as a function of time.

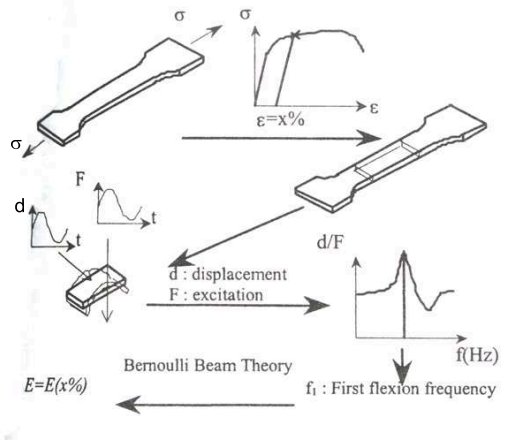

Figure 2.18: Identification method of the Young's modulus variation.

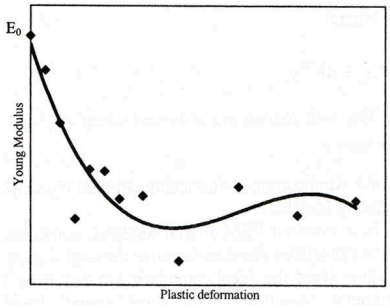

Figure 2.19: Young's modulus versus plastic deformation.

curve at initial elastic deformation and unloading curve after the given plastic deformation. The found evolution of the elastic modulus is shown in figure 2.20.

Probable reasons for the decrease of elastic modulus are the increase of micro cracks and variation of dislocation structure inside the specimen. The amount of micro cracks increases with the plastic deformation and therefore the density of the specimen decreases, which results into the decrease of elastic modulus. However, since the reduction of density due to the plastic deformation is less than 1%, its effect on elastic modulus should therefore be much smaller comparing with the one shown in figure 2.20.

Movable dislocations are considered to be the major cause of such evolution of Young's modulus, where the pile-up of dislocations due to the plastic deformation causes the decrease of the apparent elastic modulus [45]. During deformation, the released dislocations move along the same slip surface and easily pile up , when stopped by solutes, grain boundaries or some other obstacles. These movable pile-up dislocations can move backward when the shearing stress is released during unloading, leading to a small amount of non-elastic deformations. If the pile-up of dislocations occurs near the boundary of crystalline grains, the movable dislocations exist near the boundary with higher possibility than in any other

regions. Therefore, the elastic modulus may have different values within a grain. This hypothesis was confirmed by nano-indentation test. As shown in figure 2.21 the elastic modulus near the boundary has a smaller value than that in other regions.

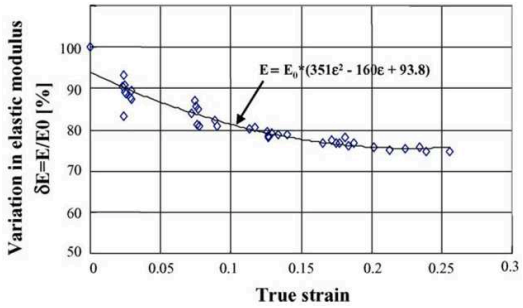

Figure 2.20: Elastic modulus variation as a function of plastic strain.

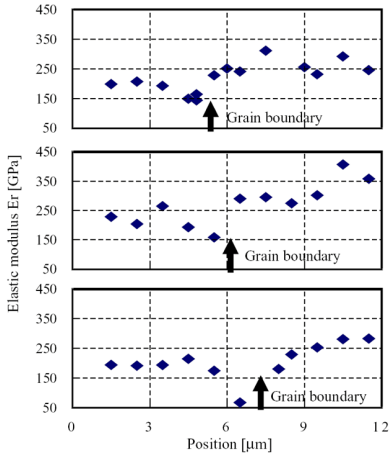

Figure 2.21: Distribution of elastic modulus within the grain.

2.2.3 Modelling of change of elastic modulus

Due to lack of reliable models most of the finite element codes used in analysis of sheet metal forming ignore inelastic effects and assume that during unloading the strain recovery is linear. As was discussed earlier, the plastic deformation in the sheet material results into an appreciable reduction of the elastic modulus and this change has a noticeable influence on the recoverable strain after forming. Some authors suggest that, if the inelastic effects are incorporated into a finite element code, accuracy of springback prediction can be improved considerably [34, 42, 43, 44, 45, 46, 47, 48]. Variation of Young's modulus in finite element analysis of sheet metal forming can be represented by: simple piecewise linear function [42,47]; power law [46,48] or higher order polynomials [45]. Authors in [49] studied the influence of variation of elastic modulus on the springback prediction. The scaled down car roof, shown in figure 2.22, was used in this study.

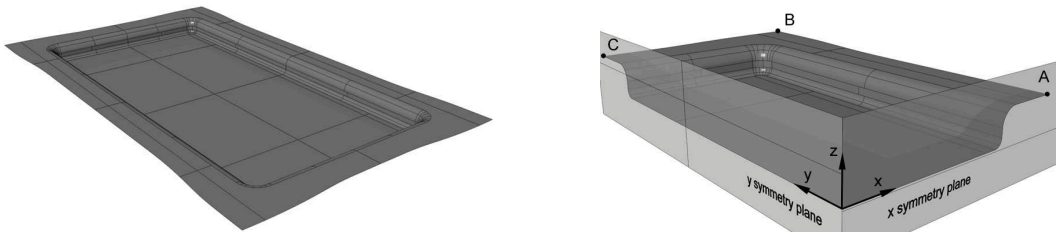

(a) final product shape

(b) measuring planes

Figure 2.22: Scaled down car roof.

Variation of the elastic modulus was roughly approximated by performing the forming step

of the simulation using the initial elasticity modulus and performing the springback step using the decreased value. The results of several simulations are presented in figure 2.23. The shape of the scaled down car roof after springback in both symmetry planes is shown

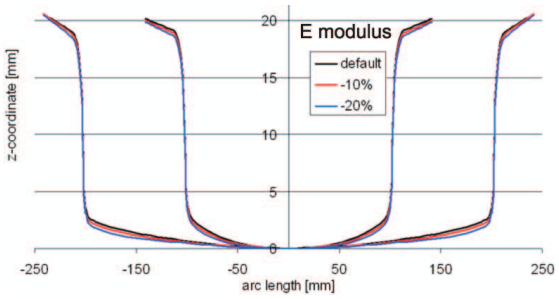

Figure 2.23: Z-coordinate as a function of the arc length along the symmetry planes of the product.

in this figure. It can be seen that with the decrease of the elastic modulus the shape in the bottom of the product changes considerably.

Recent studies of inelasticity of metals indicate that the decrease of Young's modulus of a material is strongly dependent upon the deformation path and the crystallographic texture evolution [20, 50]. The conclusion is based on the fact that inelastic deformation after unloading is caused by viscous dislocation motion driven by local internal stresses. The local internal stresses are initiated by the pile-ups or grain incompatibility effects which depend on the loading path. To accurately describe the inelastic deformation upon unloading various physically-based or phenomenological models can be used [20].

It is worth mentioning that a material can experience elastic anisotropy which involves the dependence of the elastic modulus on the rolling direction in the plane of sheet material [50]. For a rolled copper sheet (80% of thickness reduction) the Young's modulus varies by 10% (see figure 2.24). The elastic anisotropy may be yet another reason of the inaccuracy of springback prediction and needs to be taken into account.

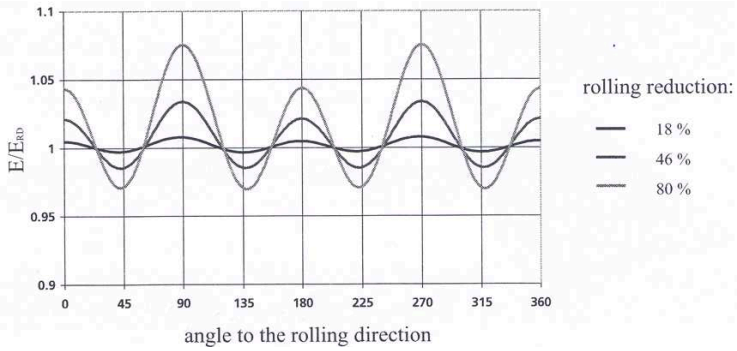

Figure 2.24: Anisotropy of elastic modulus depending on the rolling direction. Texture simulation of the rolling process of copper [48].

2.3 Characterisation of material behaviour

The choice of an appropriate material model is one of the crucial steps in accomplishing an accurate stress state. Material modelling can be divided into two parts: a part that describes the stress state of initial yielding of the material (yield function) and a part that describes how the yield function develops after plastic deformation (hardening function). In stress space, the yield stresses are graphically represented by the yield surface.

2.3.1 Description of material yielding

The first yield function was proposed by Tresca in 1864, expressing that yielding occurs when the maximum shear stress reaches a critical value. Later, based on the observation that hydrostatic pressure cannot cause plastic straining of the material, von Mises proposed a yield criterion, which is based on the experimental data provided by the uniaxial tensile test. The von Mises yield criterion for a three-dimensional stress state reads:

$$\phi = \sqrt{(\sigma_{xx} - \sigma_{yy})^2 + (\sigma_{xx} - \sigma_{zz})^2 + (\sigma_{yy} - \sigma_{zz})^2 + 6\tau_{xy}^2 + 6\tau_{xz}^2 + 6\tau_{yz}^2} - \sqrt{2}\sigma_{un} = 0 \quad (2.4)$$

Where σ_{un} is the uniaxial yield stress. The Tresca and von Mises yield functions were developed to predict yielding of isotropic materials. However, it is known that the properties of metal depend on the chosen direction and that the plastic anisotropy is the result of different features of the material microstructure, such as [51]:

- the distribution of grain orientations or crystallographic texture. The plastic deformation occurs mainly by glide of dislocations, which takes place on given crystallographic planes and in certain directions;
- the grain shape, which influence the way of interacting between different grains, and thus promote certain crystallographic slip planes and directions;
- second phases of multi-phase materials may contribute to plastic anisotropy;
- inhomogeneity of material and the presence of microstructure gradients, especially in the thickness direction.

The anisotropy of material is represented by the R-value, which is the ratio between the width strain and thickness strain defined in the uniaxial tensile test. In 1948 Hill proposed a quadratic yield function for anisotropic materials as an extension of the von Mises yield criterion. The Hill'48 yield function in general form is represented by equation 1.3. Figure 2.25 shows the yield surfaces corresponding to Tresca, von Mises and Hill'48 yield criterion.

Later the non-quadratic yield functions were proposed by Hill, Hosford, Barlat and some other authors. For example, Barlat in 1991 presented a non-quadratic yield criterion that was able to take into account the data from various multi-axial tests. For a general three dimensional stress state the yield function includes 8 material parameters, determined from various experiments. If the plane stress state situation is assumed, then the amount of

material parameters is decreased to 5 and the function can be represented by the following expression [52]:

$$\phi = (S_1 - S_2)^m + (S_1 - S_3)^m + (S_2 - S_3)^m = 2\sigma_y \tag{2.5}$$

Where S_1, S_2, S_3 are the principal values of the symmetric matrix:

$$S = \begin{bmatrix} \frac{1}{3}\Big(c(\sigma_{xx} - \sigma_{yy}) + b\sigma_{xx}\Big) & h\tau_{xy} & 0 \\ h\tau_{xy} & \frac{1}{3}\Big(a\sigma_{yy} - c(\sigma_{xx} - \sigma_{yy})\Big) & 0 \\ 0 & 0 & -\frac{1}{3}\Big(b\sigma_{xx} + a\sigma_{yy}\Big) \end{bmatrix} \tag{2.6}$$

Where a, b, c, h and m are the material parameters. The comparison between Barlat'91 and von Mises yield surfaces is given in figure 2.26. Barlat yield surfaces for various m values are also shown in this figure.

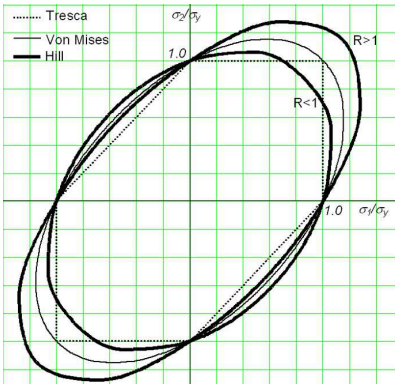

Figure 2.25: Tresca, von Mises and Hill yield surfaces in the principal stress space.

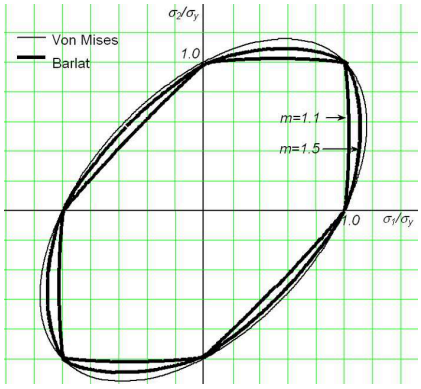

Figure 2.26: Barlat and von Mises yield surfaces in the principal stress space.

There are also some other yield criteria proposed on the basis of various principles. For example the Vegter yield function is based on experimental data obtained from the shear test, the uniaxial test, the plane strain test and the equi-biaxial test [53, 52]. Bezier interpolation of experimental data points is then used to obtain the first quadrant of the yield locus.

Accurate prediction of springback by either finite element analysis or analytical approach depends on the accuracy of the internal stress distribution within the sheet material. It is obvious that in order to increase the accuracy of the finite element simulations the yield function should be able to accurately capture all the important anisotropy effects in the material [54, 55]. The plastic anisotropy causes directional dependency of the yield stress and the R-value. As was discussed earlier sheet metals usually exhibit a certain initial plastic anisotropy which may evolve further during subsequent deformation. The evolution of plastic anisotropy during forming is called deformation-induced anisotropy and is caused by the evolution of the crystallographic texture. Deformation-induced anisotropy results in a distortion of the shape of the yield function at a macroscopic scale. If phenomenological models are used to capture this effect polynomial yield functions with hardening tensors up to sixth order are needed [48]. Unfortunately many extensive experiments are necessary

to determine the needed parameters, which makes this approach very time-consuming and cost intensive. An alternative way to capture the deformation-induced anisotropy is to use polycrystal models that are able to predict the rotation of individual grains. The implementation of deformation-induced anisotropy in the finite element analysis can be rather complex. Furthermore, complete modelling of plastic anisotropy can be very time consuming and computationally expensive [55, 56]. Therefore, in sheet metal forming, in order to simplify the analysis, it is very often assumed that the change of anisotropic properties during forming is small and negligible when compared to the initial material anisotropy [55].

Numerous studies were performed to compare the performance of different yield criteria [53, 54, 55, 57, 58, 59, 60]. It is important to mention that if a material model is able to closely describe the anisotropic behaviour observed in monotonic uniaxial tensile tests, it may be unable to predict material behaviour in other deformation conditions [58]. Authors in [54,57] emphasised the fact that in order to obtain high accuracy of the stress state after forming the yield function must contain a sufficient amount of material parameters. In addition, material characterisation needs to be done on the basis of several experimental procedures, including, for example, equi-biaxial or shear tests. In case of plane stress, the widely used Hill'48 anisotropic yield criterion contains for plane stress situation only three parameters (see equation 1.4) that are used to fit the yield function to experimental data. This lack of parameters leads to insufficient accuracy of description of directional dependency of yield stresses and R-values.

Figure 2.27 shows a comparison of the Hill's anisotropic yield criterion and the CB2001 yield function which is the generalisation of the Drucker's isotropic yield criterion to orthotropy [57]. The CB2001 yield function requires 18 material parameters for the case of a fully

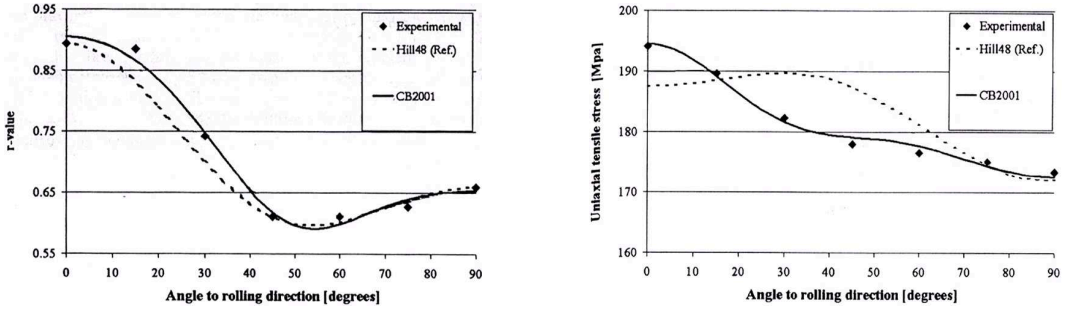

(a) r-values (b) uniaxial tensile stress

Figure 2.27: Anisotropy of uniaxial tensile stress and R-values for 6111-T4 aluminium alloy.

three dimensional stress state. In figure 2.27 the variation of experimental and predicted R-values and uniaxial tensile yield stresses with respect to the rolling direction are shown. The advantage of using an increased amount of material parameters is clearly seen, since the CB2001 yield criterion predicts the anisotropy of the yield stress and the R-values more accurately. However, the increased complexity of parameters' identification procedure may become the formidable obstacle in using the yield criterion.

The constitutive models based on a quadratic yield function are often not accurate enough and the use of more sophisticated, non-quadratic yield functions is required. Researchers in [60] investigated the influence of the initial shape of the yield function on the simulation results. In the study the Barlat-Lian yield criterion, the von Mises and the Hill'48 yield criteria were used to describe yielding of aluminium alloy. The Barlat-Lian is the non-quadratic yield function, which includes several parameters obtained from pure shear test. When considered yield functions are plotted together (see figure 2.28), one can see that they show considerable differences in the equi-biaxial point. In particular, the Hill'48 criterion has lower yield stress value for these conditions than the Barlat-Lian criterion. The Hill'48 yield function predicts an equi-biaxial yield stress lower than uniaxial yield stress. Whereas experiments show a larger equi-biaxial yield stress than the uniaxial yield stress for a material with R-values lower than 0.65. It is known as the anomalous behaviour of aluminium sheet and it is clear that the Hill'48 yield function is not well suited for describing yielding of aluminium alloys [61]. In the pure shear point the Barlat-Lian yield function has lower stress values than Hill'48. Ultimately this means that due to higher yield stresses in the pure shear point for the Hill'48 criterion the plastic deformation will be initiated later and therefore the accuracy of the state variables after forming can be arguable. Authors in [53] used limiting dome height test (NUMISHEET'96 benchmark

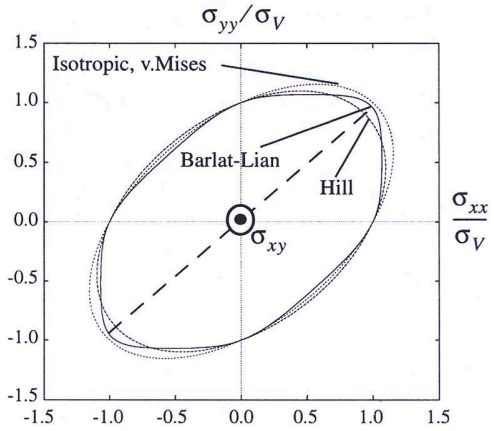

Figure 2.28: Initial shapes of aluminium alloy obtained by several yield criteria.

problem, see figure 2.29) to study the accuracy of simulation results produced by the isotropic Hill'48 yield criterion, planar anisotropic Hill'48 yield criterion and the Vegter yield function. Figure 2.30 illustrates the Vegter and anisotropic Hill yield surfaces in the principal stress space. In spite of the fact that both of the yield functions have similar average uniaxial yield stress and R-value, the shapes are different to a large degree.

Some of the results of this study are shown in figures 2.31(a) and 2.31(b), where the major and minor strains are plotted along the x-axis of the blank. It can be seen that the results of simulation with the Vegter yield function compare very well with the experimental data. The material, situated on the x-axis of the blank, undergoes the deformation regime, which lies between the uniaxial point and the plane strain point. Therefore the accuracy of the position of the plane strain point defines the accuracy of the stress state after

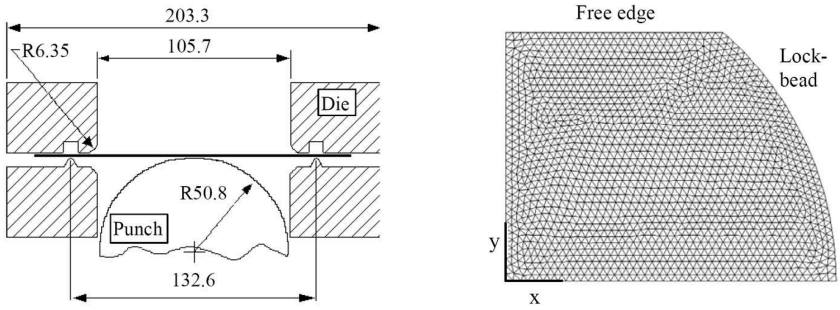

(a) schematic of the set-up (b) shape of the blank quarter

Figure 2.29: Limiting Dome Height - Numisheet'96 benchmark problem.

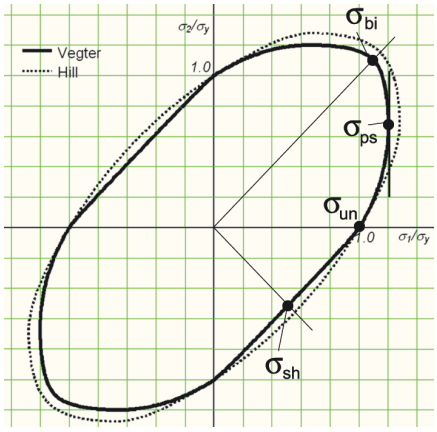

Figure 2.30: Hill and Vegter yield surfaces in the principal stress space.

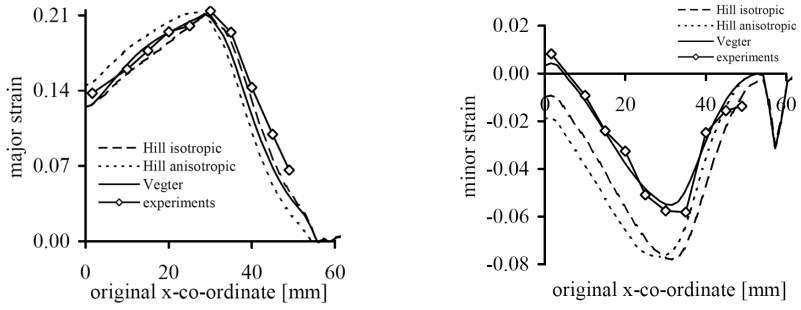

(a) major strain (b) minor strain

Figure 2.31: Major and minor strains along the x-axis (see figure 2.29(b)).

the deformation. Thus, the fact that the Vegter yield criterion was constructed using experimental values of the plane strain point and the uniaxial point is beneficial for the simulation results.

2.3.2 Description of material hardening

Phenomenological and physically based hardening models

It is well known that the yield stress in uniaxial loading increases upon increasing the level of plastic deformation. This phenomenon is known as material hardening. Several methods exist to analytically describe hardening. The most frequently used approach is to approximate the experimental stress-strain curve by a convenient mathematical function. Material hardening models developed by this approach are termed phenomenological models. A commonly used phenomenological hardening model is the Ludwik-Nadai relation:

$$\sigma_f = C\varepsilon^n \tag{2.7}$$

where constants C and n are known as the strength coefficient and the hardening rate respectively. The values for these constants are identified from the uniaxial tensile test. If the material is pre-strained (ε_0) then the relation 2.7 can be modified into:

$$\sigma_f = C(\varepsilon + \varepsilon_0)^n \tag{2.8}$$

These two equations are obtained from the uniaxial tensile test and only represent one dimensional deformation. To extend them to a more dimensional case, the equivalent stress and equivalent strains representing an arbitrary stress state must be used. The main disadvantage of phenomenological models is that they are valid for the cases comparable to the experimental results they are based on [61].

It is known that plastic deformation in metals results from the movement of dislocations on the active slip systems and the resistance to the dislocation movement determines the flow stress. Material hardening models that are based on physical principles of plastic deformation are termed physically based hardening models. They can be more accurate and can have a wider applicability, but the major drawback which limits their use is that some of the parameters are difficult to identify. In the ideal situation, the physically based hardening model considers the workhardening, strain rate, temperature and their interactions. For example, the flow stress can be decomposed into a strain and strain rate independent stress - σ_0, a dynamic stress - σ^* which depends on the strain rate and temperature, and finally a term σ_w which incorporates workhardening [61]:

$$\sigma_f = \sigma_0(T) + \sigma^*(\dot{\varepsilon}, T) + \sigma_w(\rho, T) \tag{2.9}$$

Commonly used expression for the relation between the evolution of the dislocation density ρ and the workhardening of the material can be expressed as follows [61]:

$$\sigma_w = \alpha G(T) b \sqrt{\rho} \tag{2.10}$$

where α is a scaling parameter of the order 1, $G(T)$ is the temperature-dependent shear modulus, b is the Burger's vector and ρ is the dislocation density.

Commonly used hardening laws

Isotropic and kinematic hardening models are usually used to describe the evolution of the initial yield surface during the deformation process.

Isotropic hardening is schematically explained in figure 2.32(a) [62]. It can be seen that the size of the yield surface increases uniformly, but its centre is fixed and the shape is unaltered. On the contrary, in the case of kinematic hardening the size and the shape of the yield surface remain constant, but its position shifts in the stress space as shown in figure 2.32(b).

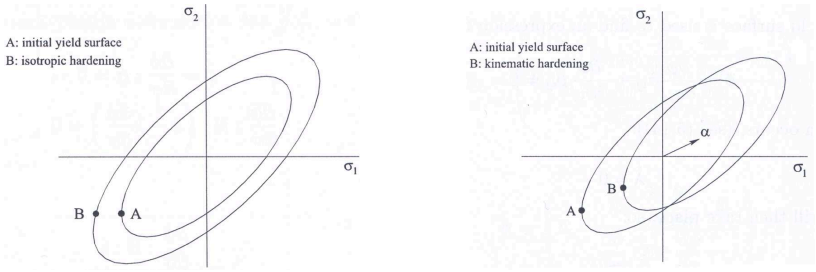

(a) kinematic hardening (b) isotropic hardening

Figure 2.32: Two extreme types of hardening models.

The stress-strain curves shown in figure 2.33 clarify the difference between both types of hardening models. If the kinematic model is used the elastic part during unloading is equal to the initial elastic part. If the isotropic hardening model is used, the elastic part increases during unloading.

(a) kinematic hardening (b) isotropic hardening

Figure 2.33: Cyclic stress-strain responses for kinematic and isotropic hardening.

Importance of the deformation history

In general, sheet material is subjected to stretch bending and subsequent unbending during forming. A typical deformation path of this type is shown in figure 2.34 [63]. Before the load reversal, point A, the hardening of the material takes place due to the movement of dislocations and their pile up at the grain boundaries. When the material passes the

bending zone, elastic unloading occurs (region between A and B). It is followed by the re-yielding of the material and subsequent change of the workhardening rate, which are caused by the motion of less stable dislocations, such as piled-up dislocations. The last two phenomenons, namely permanent softening and workhardening stagnation, are caused by the dissolution of the dislocation microstructure, formed before the unbending process, followed by the motion of dislocations in another direction and formation of new piled-up structures.

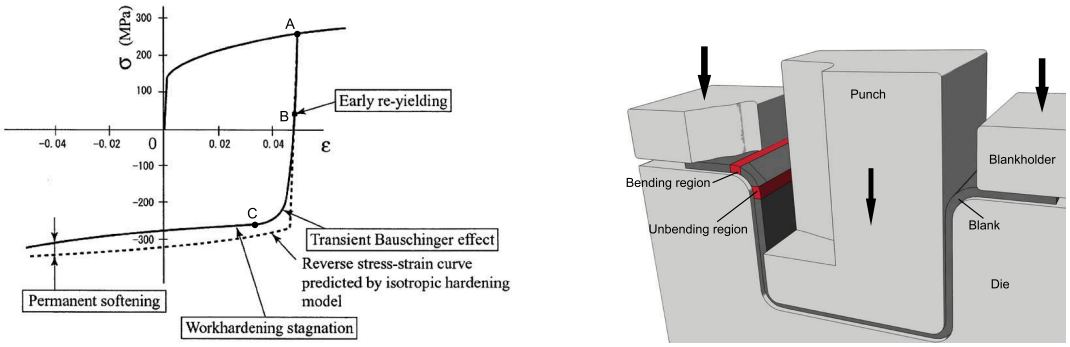

(a) stress-strain response (b) bending/unbending regions

Figure 2.34: Stages of the Bauschinger effect during cyclic deformation.

It was explained in chapter 1 that springback during unloading is caused by the internal bending moment, which is proportional to the value of the stress through the thickness of the material. Thus, it is essential that the hardening model is able to accurately describe the variation of the internal bending moment in the case of a complex deformation path. Figure 2.35 shows the schematic of the relation between the internal bending moment and curvature during bending, unbending and springback. In this example, the situations with the small and large tool radii are considered . For large curvatures (when drawn

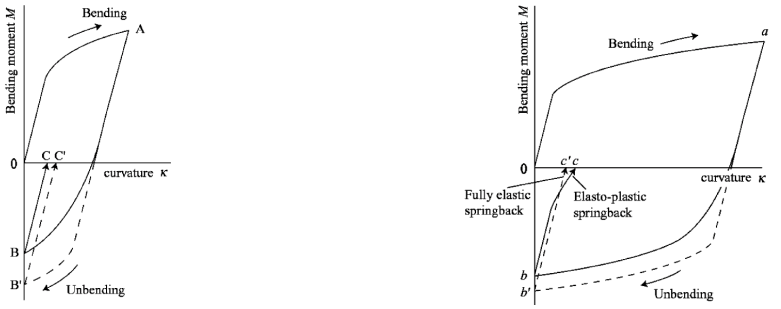

(a) large die radius (b) small die radius

Figure 2.35: Schematic of the internal bending moment-curvature relation during bending, unbending and springback processes. Solid lines represent the actual responses. Broken lines are the results calculated by isotropic hardening model [63]

.

over a small die radius), the material is subjected to severe stretch bending-unbending deformation. As a result, springback does not take place elastically, but elastic-plastically

due to the Bauschinger effect (see line b-c in figure 2.35(b). The isotropic hardening model does not take into account the Bauschinger effect and therefore springback is calculated fully elastically (see line b'-c'), which will underestimate the springback. However, in case of a smaller curvature (larger die-radius) the discrepancies in the springback results are mainly due to the overestimation of the bending moment after load reversal (see position of points B and B' in figure 2.35(a)).

Figure 2.36 shows the stress-strain curves in the case of cyclic loading of high strength steel sheet [63]. In this figure, the experimental results are plotted together with the results produced by isotropic and kinematic hardening models. It is clear that commonly used hardening models are not able to describe the Bauschinger effect, since the isotropic hardening model overestimates the real hardening of the material and the kinematic hardening model underestimates it. Accurate modelling of the material behaviour under complex

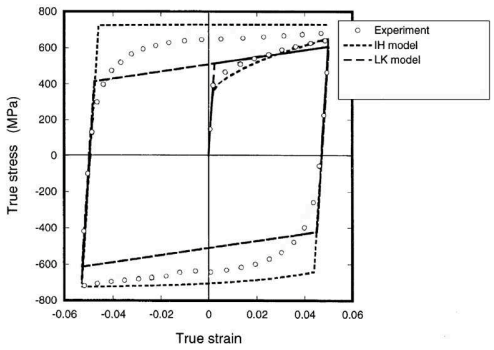

Figure 2.36: Cyclic stress-strain responses of the high strength steel sheet calculated by isotropic and kinematic hardening models.

deformation conditions with load reversals requires the hardening model to be able to take into account most of the stages of the Bauschinger effect [21,35,32,33,38,39,40,63,64,65,66].

Modelling the Bauschinger effect

It is believed that to model the Bauschinger effect properly, the following three major requirements must be addressed [33]:

- correct non-linearity of stress-strain loop;
- early re-yielding;
- permanent softening.

The fundamental framework on kinematic hardening rules was initiated by Prager and Ziegler [67, 68]. The linear kinematic hardening models developed by these authors can only provide rough approximations to the Bauschinger effect and have sharp reverse yield at fixed stresses. Based on the framework developed by Prager and Ziegler, the anisotropic hardening models were proposed by various authors, including multi-surface theory by

Mroz [69], the two-surface model by Krieg [70] and the nonlinear kinematic hardening model by Frederick and Armstrong [71]). The major difference between these models is the way of defining the generalised plastic modulus [66]. In the two-surface model proposed by Krieg and Mroz's multi-surface model, the hardening modulus function and the translation direction are defined first, then the magnitude of the yield surface translation is determined from the consistency condition. In the model proposed by Frederick and Armstrong, the direction and the magnitude of the yield surface translation are defined first, then the consistency condition is used to derive the generalised plastic modulus [72].

The hardening models developed by these authors have both advantages and disadvantages. The multisurface model is able to reproduce the abrupt change of the hardening rate after the load reversal, but at the cost of many material parameters [32]. The major problem of the two-surface model proposed by Krieg is related to the updating procedure of the distance between the current stress point and a mapping point on the bounding surface. In a complex loading situation the updating procedure can create significant overshooting problems [72]. The nonlinear kinematic hardening model proposed by Frederick and Armstrong is characterised by difficulties in modelling the smooth elastic-plastic transition after the load reversal.

All major types of hardening models received certain attention in the recent literature. Based on the framework of isotropic/kinematic hardening and Mroz's multi-surface model, Gau and Kinzel [38] proposed a hardening model that takes into account the Bauschinger effect and is able to accurately predict springback when the sheet material undergoes a complicated deformation path.

Basic concept of the Frederick and Armstrong model was extended by various authors. The main focus was given to improving the modelling, incorporating additional experimentally observed phenomena and accommodating more complex loading cases [71]. The major contribution to the modification of the Frederick and Armstrong model was done by Chaboche [73]. It was proposed to decompose the total back stress into a number of additive parts to make it possible to describe the smooth elastic-plastic transition upon the load reversal. However, the major drawback of this type of models is that the generated flow stress upon reversal saturates to the monotonic loading curve. Therefore, the permanent softening cannot be modelled.

Geng and Wagoner [66] proposed an anisotropic hardening model based on developments of Frederick and Armstrong and the modifications of Chaboche. The model consists of two yield surfaces: the active yield surface and the bounding surface. The major difference with the Chaboche implementation is that the bounding surface is allowed to develop according to a mixed isotropic/kinematic hardening law. This two-surface model is able to replicate all three principal characteristics of the Bauschinger effect.

As a good alternative to the Geng-Wagoner model, a reasonably simple anisotropic nonlinear kinematic hardening model was proposed by Chun et al. [33, 65]. It is based on the Chaboche hardening model and is able to model the Bauschinger effect consistently over multiple cycles. Modification of the Chaboche model was suggested to simplify the parameters identification procedure and to make use of conventional tensile test data for an isotropic response. The material parameters for both Geng-Wagoner and Chun's aniso-

tropic hardening models are obtained by either curve fitting of tension/compression test data [66] or using the inverse methods based on cyclic three points bend tests [32].

Some authors independently proposed hardening models of large-strain cyclic plasticity based on the framework of the two-surface hardening model developed by Krieg : Huétink et al. [40] and Yoshida and Uemori [35, 63, 64]. The Yoshida-Uemori model includes seven material parameters, which can be identified from cyclic compression-tension experiments. This model describes all the features of the Bauschinger effect, including the workhardening stagnation, and it is also able to accurately describe the strain-range dependency of cyclic hardening [64]. The last phenomenon is related to the experimentally observed dependency of cyclic stress amplitudes on cyclic strain ranges.

Huétink et al. presented a hardening model which is capable of describing deformation of sheet metal when subjected to a non-proportional loading paths. Figure 2.37(a) shows both yield surfaces plotted in the principal stress space. One of the yield surfaces is the active kinematic yield surface; another is the fictive isotropic yield surface. A hypothesis is proposed that the hardening rate depends on the distance d between the actual stress point $\underline{\sigma}$ and the fictive stress point $\underline{\sigma}_{fict}$ (see figure 2.37(a)). The slope of the stress-strain

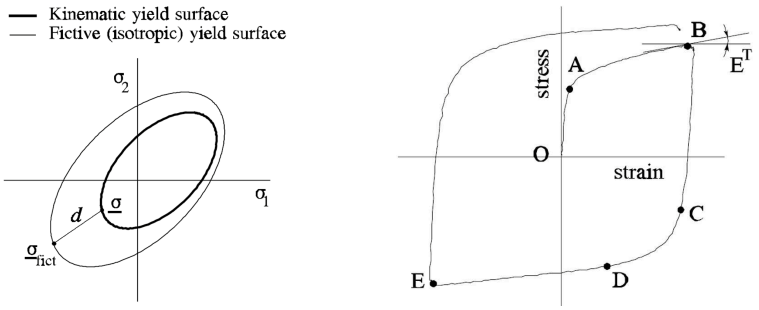

(a) two yield surfaces (b) stress-strain diagram

Figure 2.37: Two yield surfaces hardening model. Experimental cyclic stress-strain diagram.

curve after reversal of the load (region BCD in figure 2.37(b)) is formulated as follows [40]:

$$\dot{\sigma} = \Big(bE - (1-b)E^T\Big)\dot{\varepsilon} \tag{2.11}$$

where scalar b is a function of the distance d, E is the Young's modulus and E^T is the plastic tangent modulus, as defined in figure 2.37(b).

The non-proportional cyclic deformation path is shown in figure 2.40. Before the deformation starts, the active kinematic yield surface coincides with the fictive isotropic one (as shown in figure 2.38(a)). The deformation in the region AB (see figure 2.37(b)) is represented by the expansion of the fictive isotropic yield surface and the translation of the active kinematic yield surface in such a way that $\underline{\sigma}$ remains on both surfaces (as shown in figure 2.38(b)). In this case, the distance d is zero and the hardening rate is equal to the slope of the monotonic stress-strain curve. As soon as load reversal takes place, the material is elastically unloaded (region BC in figure 2.37(b)). During elastic unloading, $\underline{\sigma}$ lies inside the active kinematic yield surface as can be seen in figure 2.38(c). With increase

of the loading, $\underline{\sigma}$ travels inside the active kinematic yield surface towards the opposite side (point C in figure 2.38(c)) and plastic deformation starts again. A fast hardening occurs when $\underline{\sigma}$ moves from point C to point D (see figure 2.38(d)). When the active kinematic yield surface approaches the fictive isotropic yield surface, the hardening rate decreases. As soon as $\underline{\sigma}$ touches the fictive yield surface, the hardening is controlled only by its isotropic growth.

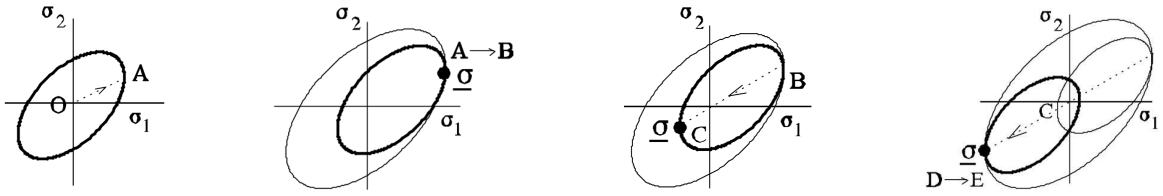

(a) initial state

(b) before load reversal

(c) after load reversal

(d) after certain amount of deformation

Figure 2.38: Schematic description of the two yield surfaces hardening.

Unfortunately, the deformation conditions in the real forming processes are very complex and the strain paths are not proportional even in single stamping operation. For a sequence of forming operations the deformation history complicates even further. To accurately describe the material behaviour under multi-axial and non-proportional loading conditions the phenomenological models are not sufficient [56, 74]. Even though the Bauschinger effect after the load reversal can be accurately described by these models, the so-called cross hardening cannot be predicted. Cross hardening can be described as an increase of the flow stress when the change of the strain path is orthogonal to the initial one. It is always possible to introduce more complicated equations with extra material parameters to improve the ability of phenomenological hardening models in describing the material behaviour under strain paths changes. However the identification of material parameters can be either very complicated or impossible [56].

The material behaviour under complex strain path changes can be described by dislocation-based anisotropic hardening models [56,75]. The models enable the simulation of the effect of complex strain path histories on the basis of the evolving dislocation structure. These type of models can be used in combination with well known yield criteria or in combination with crystal plasticity constitutive models [74]. It is clear that the industrial application of later combination needs to wait for a further progress in computer technology.

Variation of parameters of material model

The experimental material testing provides the input for a material model that is used in a finite element code. It is a common knowledge that material properties vary between different coils or even within it. Authors in [49] investigated the sensitivity of springback behaviour to variation in material properties. The simulations of forming and springback steps of scaled down car roof (see figure 2.22) were performed in the sensitivity analysis. In

the simulations the behaviour of material - forming steel $DX56D$ - was described by the Hill'48 yield criterion in combination with the extended Ludwik-Nadai hardening law. The yield stress was varied with ±10% deviation, while the C- and n-values were kept constant. 10% deviation was chosen since the yield stress is difficult to measure. The R-value was varied with ±5% deviation. The C-value was varied with ±10MPa deviation. The n-value was varied with ±10% deviation. The initial yield stress was kept constant for the last two situations, which means that the value of pre-strain ε_0 was implicitly varied. The figures below show the results of performed simulations.

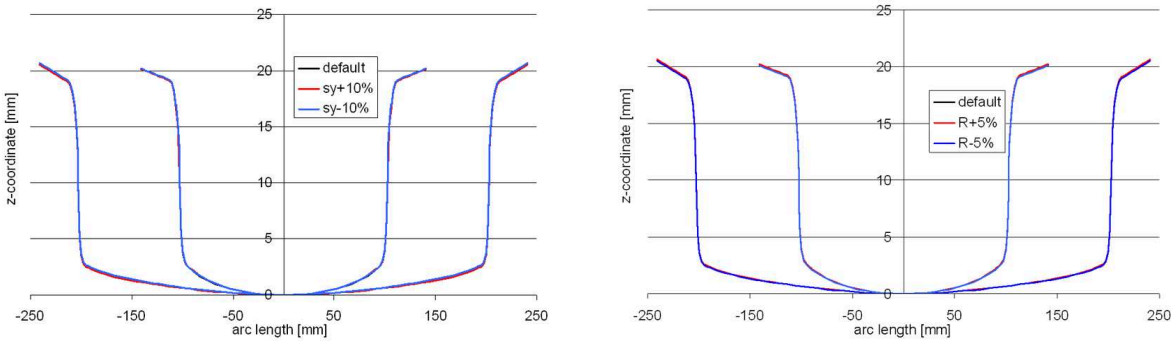

(a) variation of yield stress (b) variation of R-value

Figure 2.39: Z-coordinate as a function of the arc length along the symmetry planes (see figure 2.22(b)).

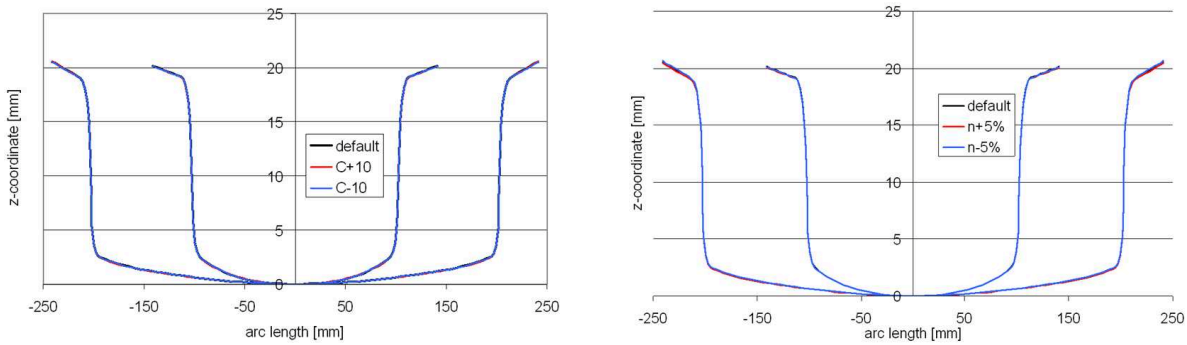

(a) variation of C-value (b) variation of n-value

Figure 2.40: Z-coordinate as a function of the arc length along the symmetry planes.

Based on these results one can conclude that the variation in material properties does not have a significant influence on the springback behaviour of this product.

Chapter 3

Springback prediction

Purely numerical factors, which influence the accuracy of springback prediction are discussed in this chapter. The chapter starts with the explanation of methods of numerical unloading. Then the selection of a time integration scheme for springback analysis is discussed. The chapter continues with the description of difficulties related to the choice of elements and the level of mesh fineness, followed by the short description of advantages and disadvantages of contact algorithms, which are used in simulations of sheet metal forming processes.

3.1 Unloading method

Simulation of springback comprises of two major steps: loading (actual forming) and unloading (springback). For the unloading procedure two methods are commonly used. In most springback analysis the instantaneous release method is employed. According to this method the change of shape of the drawn product due to the release of the tools is calculated in one increment. Sometimes this increment is subdivided into a number of sub increments to avoid numerical instabilities. During the procedure all the contact forces are suddenly removed, transformed into residual forces and then gradually reduced to zero. The material response is calculated under the assumption of fully elastic deformations in the complete model [23, 76, 77].

An alternative method can be described as inverse forming, during which the loads are reversed and the tools are gradually retracted. This method is less used since it is more computationally costly. At the same time it is more realistic because the contact forces are present during the unloading step [13, 21, 23, 78, 79].

In the study performed by Meinders et al. [23] the sensitivity of springback to the method of unloading was analysed. Unconstrained cylindrical bending (the NUMISHEET'02 benchmark problem, see figure 2.1(a)) was used due to its simplicity in quantifying springback and high sensitivity to various parameters. It was observed that the angle θ after springback can vary up to 2° depending on the unloading method used. The reason behind this discrepancy lies in the presence of tangential friction forces, which occur when tools are

physically retracted. Figure 3.1(a) shows that in the beginning of unloading, before the internal bending moment is decreased to zero, the friction between the punch and the blank will result into tangential forces pointed towards the blank centre. Since the centre of the blank (point A in figure 3.1(a)) was in compression due to bending, adding the compressive forces will promote further plastic straining upon unloading [23]. Figure 3.1(b) shows the equivalent plastic strain along the top of the sheet as a function of the current arc length along the sheet (curve through the point A, B and C). Several stages of loading (till 1.0 sec.) and unloading (till 1.1 sec.) are plotted together in this graph. It is clearly seen that the plastic strain near the point A increases as the unloading starts. This variation of internal variables during the physical unloading causes the variation of the angle θ after springback.

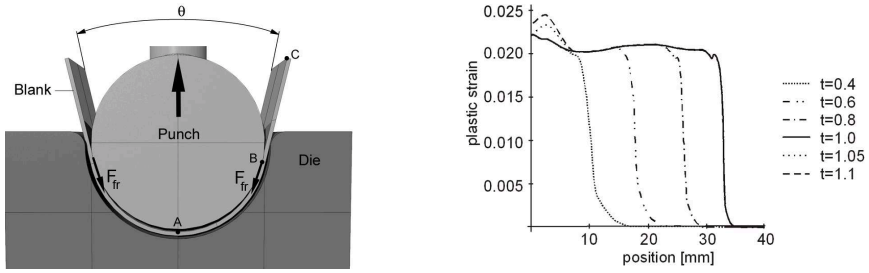

(a) contact forces (b) plastic strain evolution

Figure 3.1: Influence of contact forces on the plastic strain distribution during unloading.

No change of the plastic strain was observed for the case of the instantaneous unloading. During the instantaneous springback the described effect does not take place, the contact forces are completely neglected and therefore purely elastic unloading takes place.

Additional difficulties may arise when using the instantaneous unloading during springback step in buckling dominated problems. In a separate study performed by Meinders et al. [49] both unloading methods were used to simulate springback of the scaled down car roof (see figure 2.22). While being formed, some parts of the product flange experience high compressive stresses and tend to buckle during subsequent springback. It was observed that the instantaneous release of tools is not a good option for this type of problems, since it failed to produce the realistic product shape after springback (see figure 3.2(a)). The realistic solution can only be found when, for example, stabilisation techniques are used. On the contrary, the gradual unloading method can be considered as a natural way of controlling the buckling. When employing the gradual release of tools the amplitude of flange oscillations is controlled by the moving blankholder, which results into the expected product shape (see figure 3.2(b)).

The influence of sequence of tools' retraction on springback behaviour was also investigated in the course of this study. The unloading procedure consisted of complete or partial tools' retraction - gradual retraction of one or several tools followed by the instantaneous unloading. From figure 3.3 one may conclude that the unloading sequence can have an influence on the results. It is preferable that the tools' retraction in the simulation imitates the real unloading procedure [49]. Additionally, it can be seen that the partial gradual

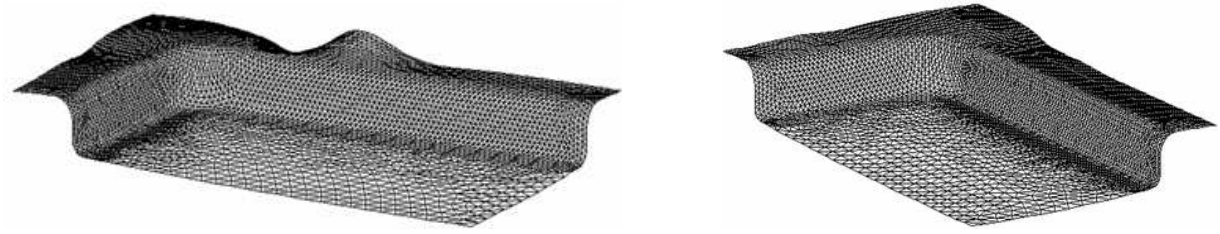

(a) final product shape - instantaneous unloading (b) final product shape - gradual unloading

Figure 3.2: Springback in buckling dominated problems.

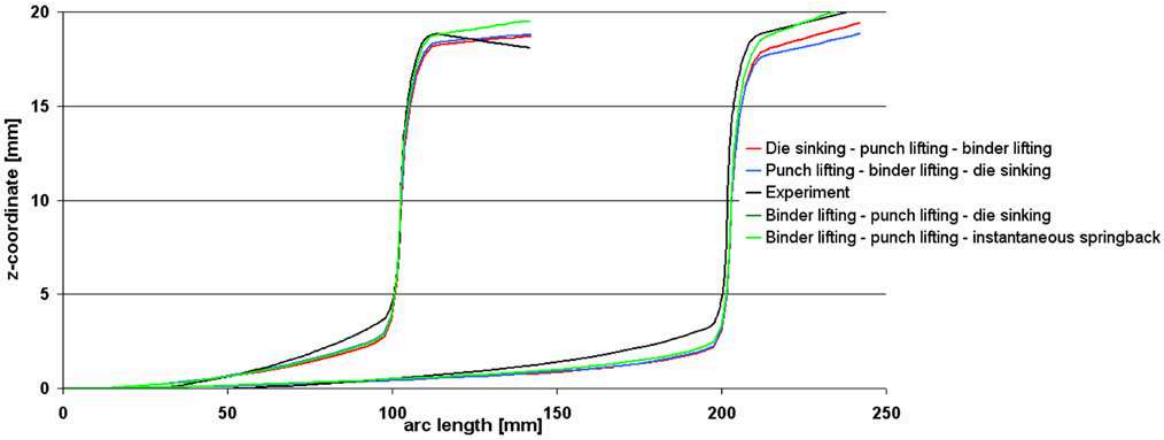

Figure 3.3: Variation of unloading sequence and its influence on springback prediction. Z-coordinate as a function of the arc length along the symmetry planes (see figure 2.22(b)).

unloading can have no influence on final results and can be used to decrease the simulation time (in figure 3.3 the lines *Binder lifting - punch lifting - instantaneous springback* and *Binder lifting - punch lifting - die sinking* coincide).

3.2 Stabilisation and damping techniques

The main disadvantage of the gradual unloading method comparing to the instantaneous unloading is the computation time. The gradual unloading requires a lot of CPU time and is very often accompanied with bad convergence behaviour of the simulation due to the presence of tools' sliding with low normal forces. To stabilise the computation stabilisation techniques or numerical damping are commonly used. The influence of stabilisation techniques on the simulation results was investigated by authors in [49]. Two stabilisation methods, namely NNGT and DSTF, were used in combination with the instantaneous and the gradual unloading. According to the NNGT method the negative contribution of the non-linear geometric terms to the stiffness matrix is neglected. The DSTF method is based on adding the extra values to the diagonal terms of the system stiffness matrix. Both methods only influence the predictor stage of the FE algorithm, therefore the final

outcome of the analysis is not influenced, provided that the unbalance criteria are strict and there is a unique solution. However, in case of instabilities, more solutions are possible, and the choice what solution path is followed depends on the predictor stage [49]. Figure 3.4 shows the results of simulations of the scaled down car roof (shown in figure 2.22(a)) when the gradual unloading method was used in combination with the mentioned stabilisation techniques. In this figure the z coordinate is plotted as a function of the arc length along the edge of the product flange (through points A, B and C shown in figure 2.22). The NNGT stabilisation technique hardly influences the simulation results. On the contrary, when the DSTF method is used the springback is severely damped. It can be seen that the waviness in the flange is slightly visible and additionally it was observed that the springback in the bottom of the product was much smaller [49].

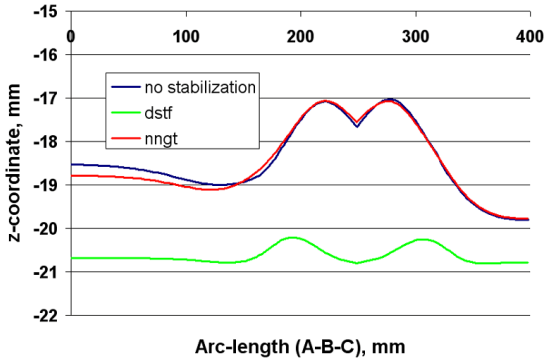

Figure 3.4: Gradual unloading with and without stabilisation techniques.

Modification of contact algorithms can be considered as an alternative solution to improve the convergence behaviour during the gradual unloading. For example, the gradual unloading can be substituted by a two-step release method. It may comprise of a release of tangential forces, followed by a release of normal force. The method may become a good approximation of the gradual unloading with low CPU time requirements [23].

To investigate whether it is possible to improve the performance of the instantaneous unloading in buckling dominated problems several simulations were performed with the NNGT and the DSTF methods. In the simulations with the NNGT method the size of the increments to reduce the residual forces to zero and the unbalance criteria were varied. Figure 3.5(a) shows the results of the simulations with 5 equal increments, 5 variable increments and 5 variable increments with strict unbalance criteria. One can see that despite the fact that the number of the increments is equal there is a significant difference in the final shape along the free edge of the product. Figure 3.5(b) shows the results of the simulations with the instantaneous unloading when the DSTF method was used. It can be seen that for low number of the increments no waviness is observed in the product flange. Furthermore, the waviness that is observed for a high number of the increments is not comparable with the shape obtained with the gradual unloading method.

Finally, several simulations were performed to evaluate the influence of the numerical damping in combination with various gradual unloading procedures [49]. The unloading

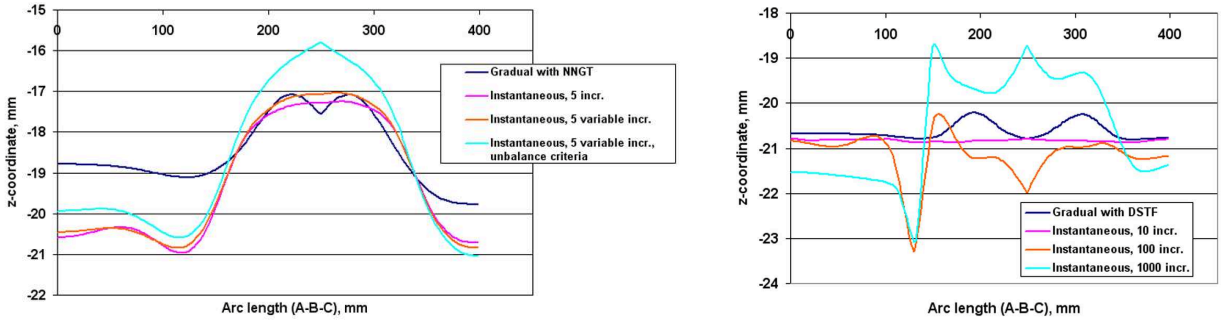

(a) NNGT stabilisation (b) DSTF stabilisation

Figure 3.5: Instantaneous unloading in combination with stabilisation techniques.

sequences are indicated in figure 3.6 where the influence of damping is shown. It can be seen that when damping is used the blank may stick to the surface of the tool during unloading and the shape of the product may become severely deteriorated. Therefore, it is important to emphasise that the use of numerical damping in springback simulations must be minimised [49].

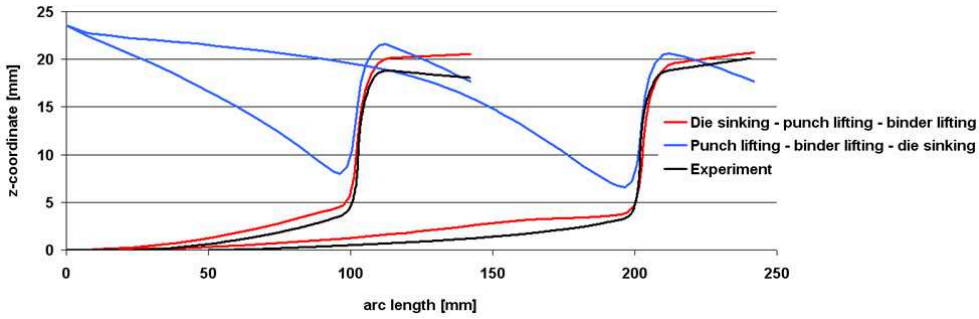

Figure 3.6: Springback simulation with damping. Z-coordinate as a function of the arc length along the symmetry planes.

3.3 Time integration schemes

There are two main solution procedures for the simulation of sheet metal forming: the dynamic explicit and the static implicit.

3.3.1 Comparison of explicit and implicit methods

The common basis of both methods is the discretized equation of motion [80]:

$$M\ddot{d} + F_{int} = F_{ext} \tag{3.1}$$

Where $\ddot{d}$, F_{int} and F_{ext} are the nodal accelerations, the internal forces and the external forces respectively. Since the internal force vector is a function of nodal displacements and accelerations, equation 3.1 is a non-linear equation in displacements, velocities and accelerations. Thus, a time integration algorithm must be used to solve this set of differential equations.

The Newmark integration method is an efficient and commonly used single-step integration algorithm. It establishes the relation between the state variables of the current state and the state to be calculated. The basic assumptions of the Newmark method are [80]:

$$d_{n+1} = d_n + \Delta t \dot{d}_n + \Delta t^2 \Big((\frac{1}{2} - \beta) \ddot{d}_n + \beta \ddot{d}_{n+1} \Big) \tag{3.2}$$

$$\dot{d}_{n+1} = \dot{d}_n + \Delta t \Big((1 - \gamma) \ddot{d}_n + \gamma \ddot{d}_{n+1} \Big) \tag{3.3}$$

Where n is the time increment and the parameters β and γ are free to choose. If $\beta \neq 0$, the displacement at time t_{n+1} is a function of its own time derivatives and the integration scheme is called implicit. An iterative procedure is needed to solve the system of equations 3.1. The second term becomes equal to $F_{int} = K u_{n+1}$, where K is the stiffness matrix. In order to iteratively solve the equations of equilibrium the computation of the stiffness matrix is required.

If $\beta = 0$, the displacement at time t_{n+1} is a function of variables from a previous step and therefore the integration scheme is called explicit. In this case the system of equations 3.1 is linear and its solution is trivial. It is important to mention that the explicit integration scheme is conditionally stable, which mean that the time increment must be less than the critical value. For linear solid elements this value can be approximated by the smallest time needed for an elastic wave to cross one element [80].

The major advantage of the explicit time integration is that it is easy and straightforward. There is no need to generate the stiffness matrix and there are no unbalance forces, since the difference between the external and internal forces determines the values of nodal accelerations at the start of every time increment. Absence of unbalance forces means that the explicit method does not suffer from the convergence problems within the time increment. The major disadvantage of the explicit integration scheme is its conditional stability and prohibitively small maximum allowable time increment. Usually to solve this problem and to decrease the total computation time mass scaling is employed. In this way the critical time increment is enlarged by artificially increasing the mass of the material.

The implicit time integration method is unconditionally stable. A time increment can be selected based on the required accuracy and the convergence behaviour. Since sheet metal forming processes are relatively slow, often the mass matrix is omitted from equation 3.1 and the equilibrium equation becomes $F_{int} = F_{ext}$. The iterative solution procedure is used to find the state variables that satisfy the equilibrium of the increment. In this way the equilibrium conditions are checked during every incremental time step giving more reliable results. The main disadvantage of this algorithm is that a linear set of equations must be solved repeatedly and the computation time for large models is significant. Difficulties in

reaching convergence within a time increment can be considered as another drawback of this method.

The popularity of the implicit method in sheet metal forming simulations is likely to increase during the next decade [80]. One the reasons is the increased fineness of the meshes used in analysis of sheet metal forming. Decreasing the size of elements of the mesh decreases the critical time step of explicit methods and thus increases the total computation time. Another reason is the increasing complexity of constitutive models, which shifts the relative simulation time from the solver part to the constitutive equation part. During implicit analysis less than 10% of CPU time is spent on evaluation of constitutive equations, whereas during explicit analysis this value is about 90% [80]. Thus physically based constitutive models in combination with small time steps may render the explicit algorithms inapplicable for realistic sheet metal forming simulations.

3.3.2 Choice of integration scheme

The sensitivity of springback to explicit/implicit solution procedures was studied by various researchers. The usual procedure is to employ the dynamic explicit method for the simulation of the forming step and the implicit method for the springback analysis [78, 81, 82, 83]. In addition to it, good results of springback simulation were reported after using only explicit analysis for both forming and unloading steps [84, 85, 86] or only implicit analysis [23, 31, 76].

One of the reasons for the popularity of the procedure, in which the dynamic explicit scheme is used during forming and the static implicit scheme is used for springback, is the critical time step. The explicit method used for springback simulation can take as long as the time spent on the forming step [80]. Furthermore, if the dynamic explicit scheme is used for springback simulation the blank may start to oscillate during unloading and therefore the final static shape of the blank is difficult to find [78]. The use of artificial damping to suppress these oscillations makes the entire procedure inaccurate and unreliable.

The application of combined explicit/implicit method for springback simulation requires a special procedure to transfer the state variables from an explicit finite element code into an implicit one [82]. Moreover, since the explicit code does not guarantee the final equilibrium of the deformed body, the applicability of the results obtained by an explicit method in an implicit springback analysis is arguable [87]. An interesting way to avoid these problems is to combine the advantages of both time integration algorithms in one finite element code. Authors in [80] proposed a method that introduces the dynamic terms into the implicit finite element code. The accuracy of the results after forming is guaranteed by the implicit algorithm. At the same time the included inertial effects decrease the simulation time and additionally stabilise the convergence procedure when iterative solvers are used.

Another interesting approach to combine merits of explicit and implicit methods was originally proposed by Jung [88] and later extended by Noels [89]. Keeping in mind the advantages of implicit and explicit schemes the optimal solution would be to have both methods readily available in the same code and to be able to switch automatically between

them in one simulation [89]. As soon as the convergence behaviour of implicit solution deteriorates during the simulation, the explicit scheme is employed. After passing the difficult point of simulation the solution strategy is switched back to the implicit algorithm.

3.4 Element types

Simulations of industrial sheet forming processes are usually performed with shell elements. The basic idea of shell elements is, that if the thickness of the structure is very small compared to its other dimensions, then its geometry is described by only using variables of the mid-plane [53]. Since only the plane of the sheet is discretized with elements the amount of independent degrees of freedom can be significantly decreased. The three major shell deformation theories can be briefly described as follows:

- *Membrane theory.* It is assumed that the bending and shear stiffness can be neglected compared to the membrane stiffness. The displacements in the entire element are approximated by the displacement of the mid-plane. The thickness strain cannot be derived from the kinematic relations and is obtained from the in-plane strain components according to the principle of plastic incompressibility. Every node of the element has three degree of freedom - three displacements.

- *The Kirchhoff theory.* The bending stiffness is taken into account. Points on the normal to the mid-plane remain on that normal after deformation. The rotational degrees of freedom are coupled with the derivative of the nodal out-of-plane displacements. Transverse shear deformations are equal to zero. The thickness strain is also derived from the in-plane strain components. Every node of the element has six degree of freedom - three displacements and three rotations.

- *The Mindlin theory.* Both the bending and the shear stiffness are taken into account. The points on the normal to the mid-plane remain on a straight line after deformation, but this line does not necessarily remain normal to the mid-surface. Transverse shear components are not equal to zero. The strain in thickness direction is derived from the principle of plastic incompressibility. Every node of the element has six degree of freedom - three displacements and three rotations.

The accuracy of a finite element solution is defined by the modelling error and the discretization error. Both errors need to be controlled in order to perform a reliable simulation. The plate theory assumptions is one of the reasons of modelling error in sheet metal forming simulations. All shell element formulations are based on the assumptions that due to geometry of the blank the plane stress state prevails and in-plane strains are linearly distributed across the thickness. It is arguable if these assumptions are fulfilled in the entire computational domain [31, 90, 91, 92, 93]. For example, shell theory is not applicable for situations when the radius of the tools is comparable with the sheet thickness. In this case the stress state will be three dimensional in nature and the strain distribution will be more nonlinear. For such situations the 3D solid elements are required. These elements

are able to accurately calculate the stress gradients in thickness direction as well as the evolution of the sheet thickness during the simulation.

Li et al. in [31] used the draw/bend test (see figure 2.4) to understand the sensitivity of springback to some of the purely numerical parameters, such as amount of integration points through the thickness, the mesh size and the type of elements. Figure 3.7 shows results of simulations for DQSK (drawing-quality, silicon-killed) steel plotted together with experimental data. In this figure the change of shape upon unloading $\Delta\theta$ is plotted versus the R/t ratio (the radius of the tool to the sheet thickness). Simulations were conducted with several element types: 2D plane stress, 2D plane strain, 3D nonlinear solid (free of shear locking) and 3D shell elements. The value of the back force (see figure 2.4) remained constant during the simulation. It can be seen from the figure that for $R/t < 6$ there is a clear departure of simulation results obtained with all 2D and 3D shell elements from the experimental data. For small values of R/t ratio the fully 3D stress state prevails and solid elements are needed to obtain accurate results [31, 93].

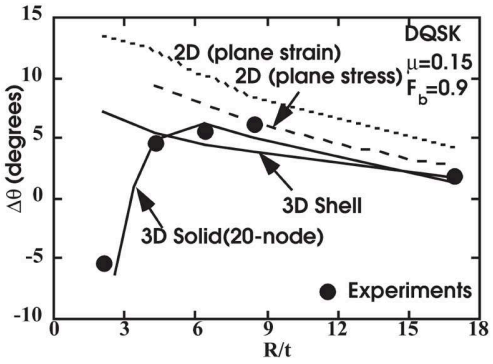

Figure 3.7: Springback ($\Delta\theta$) versus R/t ratio for different element types.

The major drawback of 3D solid elements is that they are not very suitable for simulation of complex industrial products due to enormous CPU time and memory consumption required [61]. It is known that at least two layers of solid elements need to be used to accommodate the stress gradients that occur in the thickness direction. Moreover, the ratio between the element dimensions in plane and through the sheet thickness must be small enough to avoid deterioration of the stiffness matrix [92]. Another drawback of solid elements is the presence of shear and volumetric locking phenomena, which makes the solid element behave unrealistically stiff. This problem can be resolved by employing reduced integration schemes or by using higher order elements [57, 91, 92].

The most commonly used approaches to control the discretization error are h- and p-refinement. During h-refinement the mesh is locally or globally refined, when the original mesh is no longer able to accurately describe the geometry or the steep variation of internal variables. p-refinement procedure includes increasing the polynomial degree of the interpolation function while keeping the finite element mesh unchanged. When using higher order interpolation functions, less elements is needed to describe the steep variation of internal variables [94]. The advantages of using higher order elements for springback simu-

lation were discussed by Muthler [90]. In the study the 3D solid elements with higher order interpolation or shape functions were employed (see figure 3.8). These elements allowed choosing the polynomial degree in thickness direction differently from that in in-plane direction. In addition, it was suggested that the elements with curved boundaries (see figure 3.9) can help to reduce the amount of elements used to describe the complex geometry of the structure [90].

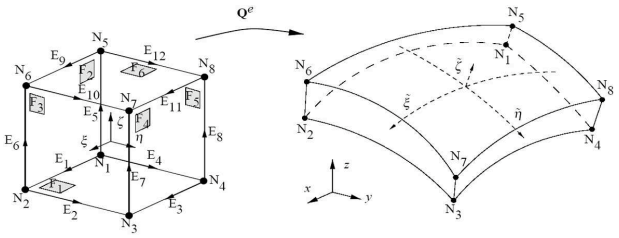

Figure 3.8: High order, curved, shell-like solid element.

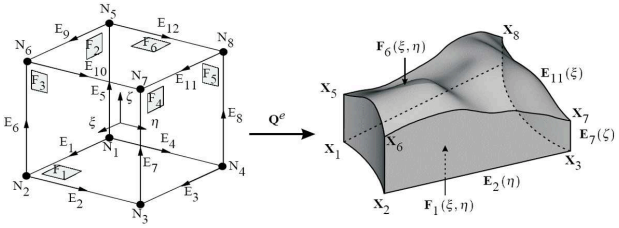

Figure 3.9: Curved side of the high order shell-like solid element.

However, the main shortcoming of using higher order elements is that they are computationally expensive and their implementation is less straightforward.

Another interesting approach, which makes use of advantages of shell and solid elements was proposed by Xia et al. [95]. It was suggested to use solid elements in the regions of the blank which may experience fully three dimensional stress state, and shell elements in the remaining part of the blank. A solid-shell transition element was developed to ensure the compatibility and continuity of both deformation and traction along the shell-solid interface. It is important to mention that the method was applied for flanging problem and the mixed mesh was created beforehand. In realistic simulations of sheet metal forming the material flows over regions with sharp geometry, and the fully three dimensional stress state occurs at various blank locations. Therefore, it is very problematic to identify in advance the exact locations of solid elements and an algorithm, which transforms the shell elements into solid elements and vice versa during the simulation is needed.

3.5 Tools description and blank discretization

As was discussed earlier, the accuracy of a finite element solution is influenced by the discretization error. The realistic results of a simulation can only be obtained if the mesh

sizes of a blank and tools are chosen correctly. It is suggested, that accurate springback simulation requires more nodes on the tool radius than usually recommended for forming analysis [21,23,31,46,87,94,93]. Based on the results of simulations of the draw/bend test (see figure 2.4) authors in [21] concluded that for satisfactory results one node per 5° of turning angle of the tool radius is required.

The influence of mesh sizes on the springback behaviour of the scaled down car roof (see 2.22) was studied by Meinders et al. [49]. Several simulations were performed in which the mesh fineness was changed initially or during the simulation. The obtained results were compared to the outcomes of the simulation with a default mesh. When the default mesh was used the punch and the die radii (5.0mm and 10.0mm) were covered with 4 and 6 plate elements respectively. In the simulations, which are referred later as "sim_ref1" and "sim_ref2", the elements were allowed to refine once and twice correspondingly. During adaptive mesh refinement each element was equally divided into 4 elements which means that every refinement level led to a doubling of the elements over the tools' radii. This resulted in 8 and 12 elements covering the punch and the die radii respectively after the first level of refinement. After two levels of refinement the punch and the die radii were covered with 16 and 24 elements correspondingly. In the simulation which is later referred as "sim_fine" the initially fine mesh was used. The size of the elements covering the tools' radii was comparable with the elements' size after 1 level of mesh refinement.

The experimental and simulation results are shown in figure 3.10. When looking at the shape of the product in x and y symmetry planes it can be concluded that the springback is overestimated when using the default mesh. The results of the simulation with one level of mesh refinement show a good resemblance with the experiments if looked at the z-position of the product corner. On the other hand, the curvature in the bottom is larger than that observed in the experiments. Further refinement shows an underestimation of the springback behaviour, namely both the z-position of the product corner and the curvature in the bottom do not resemble the experimental results. However, it can be seen that refining the elements leads to converging results [49].

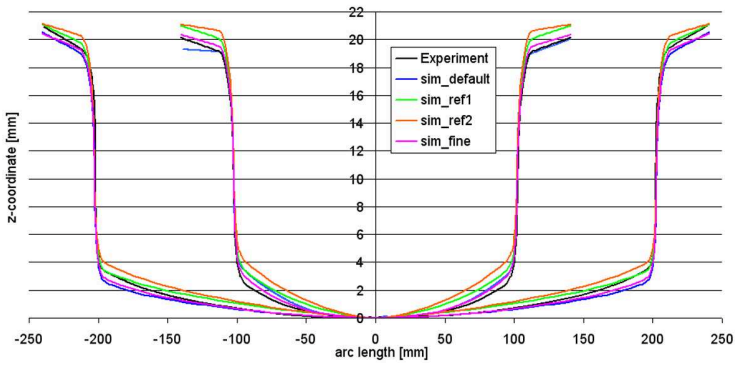

Figure 3.10: Z-coordinate as a function of the arc length along the symmetry planes (see figure 2.22).

Figure 3.10 also shows that the results of the simulation with the initially fine mesh are in better agreement with the experiments than those with the default mesh. However,

the springback is still overestimated. It is important to mention, that the results of the simulation with the initially fine mesh and the simulation with one level of mesh refinement differ significantly, despite the fact that the elements of both simulations at the end of the forming step were comparable in size. This fact suggests that, in addition to the dependency of springback behaviour upon the mesh sizes, the mesh refinement procedure may also have a considerable influence [49].

Due to complexity of the product geometry very often the tools' surfaces are discretized, instead of being described analytically. Thus the amount of elements needed to discretize the tools' surfaces is as important as the amount of elements comprising the mesh of the blank [23]. A small number of elements describing the tool radius may generate the situation when the tool surface becomes rather sharp with respect to the blank surface. Figure 3.11 shows the die radius discretized with 3 and 20 elements. When only three elements are used the "artificial" sharp edges of the tool will produce the additional restraining force acting on the blank, which will modify the stress state after forming and influence the accuracy of springback prediction. [23]. On the contrary, 20 elements over the die radius are able to represent the original smoothness of the surface (see figure 3.1(b)).

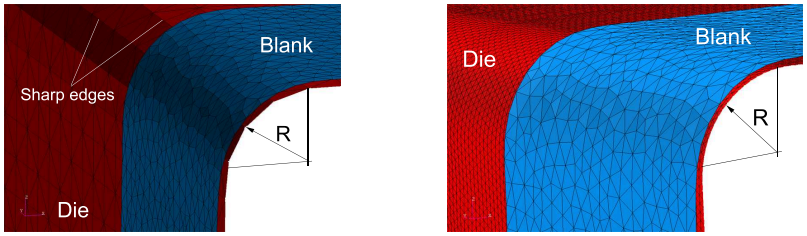

(a) rough tool surface (b) smooth tool surface

Figure 3.11: Examples of discretization of die radius.

Figure 3.12 shows the results of several simulations of S-rail section (NUMISHEET'96 benchmark). In the simulations 3, 12 and 48 elements over the tool radius were used [96].

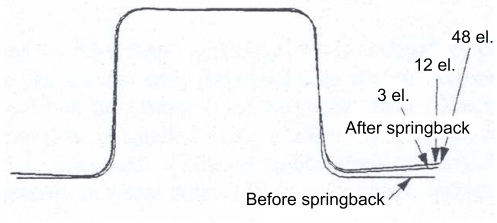

Figure 3.12: Influence of tool discretization on springback

It can be seen that the springback amplitude in case of only 3 elements over the die radius is lower comparing with 12 and 48 elements. The rough mesh over the tool radius produced an additional tension acting on the blank, which decreased the amount of springback.

It is important to emphasise that the attempts to utilise the analytical description of forming tools in analysis of sheet metal forming are still performed [97, 98]. In spite of

plenty of difficulties related to the data transfer between CAD and CAE packages and the necessity of modifying the contact strategies, analytical surfaces can give the most accurate description of tools and can make the tedious meshing step needless.

The subject of tools and blank discretization is not sufficiently described in the recent literature and therefore an additional study needs to be performed to investigate the sensitivity of springback to mesh sizes.

3.6 Description of contact

In sheet metal forming the contact conditions are usually described based on the following considerations [99]:

- the material cannot penetrate the tool and if there is a contact, the gap between the material and the tool is zero;
- if there is no contact, then no contact forces can occur, and therefore the product of the gap and the contact pressure is always zero.

Lagrange multiplier method and penalty method are the main methods used to incorporate the contact conditions into a finite element formulation. An extensive description of both methods can be found in [53, 99, 100]. Briefly, according to the Lagrange multiplier method the non-penetration contact conditions are considered as extra equations. They are incorporated in the system by multiplying these conditions and the multiplier becomes the contact pressure [99]. The non-penetration conditions are exactly enforced by this method, but at the cost of extra degrees of freedom.

According to the penalty method the non-penetration conditions are weakly enforced and the penalty is viewed as a contact stiffness. The major advantage of the method is that no extra degrees of freedom are required. There is always a small amount of penetration and if no penetration is required then an infinite contact stiffness is needed. However, a high value of contact stiffness introduces stability problems. During the simulation the non-linear change of contact occurs. High contact stiffness will result in high contact forces which will destabilise the convergence of the simulation. This in return will require small incremental steps to keep the calculation stable if changes in contact may occur. On the contrary, the Lagrange multiplier method with smaller values of contact stiffness offers extra advantages from the point of view of the simulation stability.

Both methods are equally frequently used in simulation of sheet metal forming and springback [101, 84]. If some geometrical inaccuracy is acceptable, thus a small amount of penetration is allowed, the penalty method is preferable due to its CPU cost advantage. Furthermore, allowing a small penetration or modelling the tools as deformable bodies gives an extra advantage - reduction of discretization error by making the contact between the blank and the tool more smooth. Meinders et al. [23] analysed the influence of chosen contact strategy on springback based on the simulations of the cylindrical bending problem (see figure 2.1(a)). Figure 3.13 shows the force displacement curves obtained from the

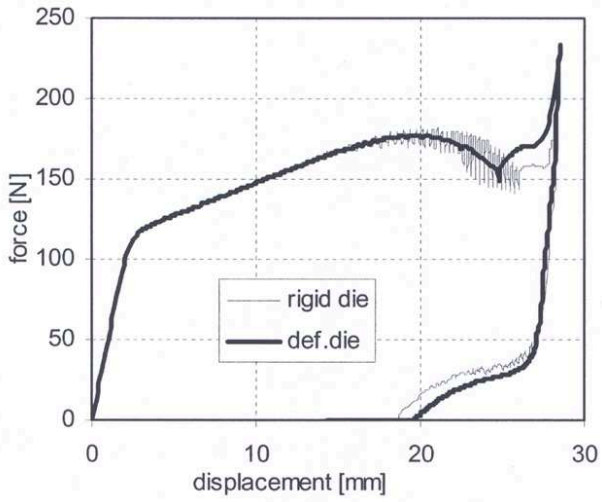

Figure 3.13: Cylindrical bending. Punch-force displacement curves for rigid and deformable dies [23].

simulations with rigid and slightly deformable tools. It can be seen that one of the curves contains a periodic disturbance and their shapes are different. The periodic disturbance is caused by the discretized blank passing the rigid die radius. The variation of the shapes of the curves can be explained by the discretized die restraining the blank, when it passes the die radius. A local refinement of the blank and die meshes can help to reduce the observed disturbance and shape variation, but the influence of the discretization error will remain. An alternative and more practical way to suppress the oscillation and to get rid of artificial restraining forces acting on the blank is to model the die as a deformable body. The advantage of the last approach is that it is computationally less expensive and a much more stable situation can be obtained [23].

It is worth mentioning that an appropriate description of friction is very important for obtaining realistic forming conditions and an accurate stress state [19]. Firstly, as was shown in several studies, the accuracy of springback prediction is very sensitive to the used value of the coefficient of friction [23, 49]. Secondly, a commonly used Coulomb friction model assumes a constant coefficient of friction, whereas it does not entirely correspond to reality. The coefficient of friction depends on the local contact conditions, which differ for each sheet/tool contact. There are several different contacts between the sheet and the tools for each forming process and therefore a more complex friction model is required. The Stribeck friction model takes into account the variation of the coefficient of friction depending on the contact conditions. According to this model the coefficient of friction depends on the pressure, viscosity of a lubricant between the contacting surfaces, the sum velocity and the roughness of the two surfaces.

Chapter 4

Springback reduction and compensation strategies

The automotive and other manufacturers of sheet metal parts rely on several methodologies to control springback, namely, mechanics-based reduction and geometry-based compensation [3]. The mechanics-based reduction methodology is based on physics of the springback phenomenon. The amount of springback is reduced by changing or constantly varying the process parameters. Geometry-based compensation is used to change the die geometry so that the sprung back shape of the product matches the target shape. Both methodologies are briefly discussed below.

4.1 Springback reduction

The mechanics-based reduction methodology relies on the mechanics of sheet metal forming, which becomes the basis for identifying and modifying the critical process parameters at the critical time intervals to control the amount of springback. There are several commonly used methods:

- *Blankholder force control.* The method is based on increasing or decreasing the binder force during forming, and thus increasing or decreasing the tension in the sheet material. Various studies were performed to clarify the method of acquiring the best trajectory of the blankholder force during forming [28, 102, 103, 104]. The blankholder force trajectory is selected, if it allows to decrease the springback by increasing tension in the material (see section 1.1.4) and to decrease the chance of fracture appearance.

- *Through thickness deformation.* In this method the springback is decreased by deforming locally certain regions of the blank (see figure 4.1). The regions should be selected accurately, since local through-thickness deformation must be applied to the regions with maximum internal bending moment [24].

- *Forming in multiple steps.* Forming of a product is performed by means of several tool sets or by means of one tool set with some additional mechanisms. Typical examples of this type of operations are redrawing, forming with reconfigurable tooling [105] or "bottoming" [24]. The process of "bottoming" is shown in figure 4.2. The major idea behind the method is to use the springback caused by making the bottom curved to compensate the amount of springback in the wall. Reconfigurable tools are made of a large number of metallic pins with convex tips, as shown in figure 4.3. Their height can be adjusted to represent any shape of the final product or to control the amount of springback. To produce high surface quality there is a thick layer of polymer between the blank and the tool.

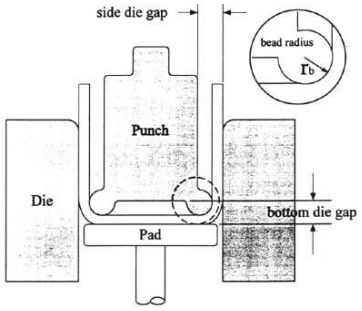

Figure 4.1: Principle of through-thickness deformation method.

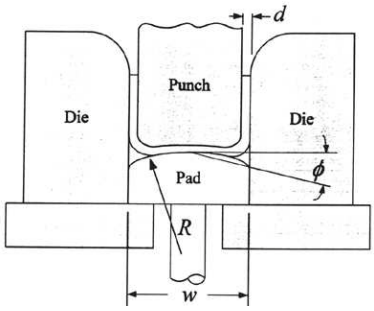

Figure 4.2: Forming with multiple tool movements.

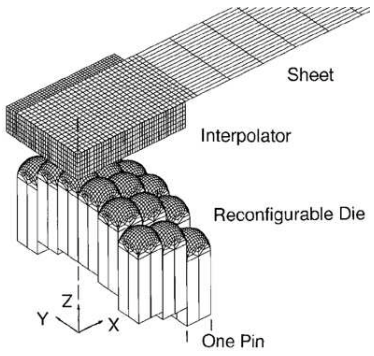

Figure 4.3: Forming with reconfigurable tools.

4.2 Springback compensation

The geometry-based compensation methodology can guarantee the shape accuracy of the formed product by performing the appropriate modifications of the tools. The basis of modification of the tool geometry are the results of simulations or the measurements of the part after real forming. The are several methods available for shape compensation:

- *Spring forward.* According to this method the forces acting on the tools at the end of forming stage are identified. These forces are applied to the target geometry and

an elastic finite element simulation is performed. The shape obtained in the end of simulation is considered to be the required shape of the tool, which can compensate springback [77, 106]. It can occur that the desired shape is not obtained after the first calculation. In this case the procedure is repeated with the new forces, obtained from a new simulation with the tools' shape obtain after first iteration. The algorithm continues until there are no deviations from the desired shape of the product or the deviations are within the specified error.

- *Displacement adjustment.* According to this method the difference between the target and obtained shapes is calculated first. The obtained displacement field is multiplied with a certain compensation factor. This results in a compensated geometry of the tools. The compensation factor depends on the geometry of the product and its material. Based on the results of the first iteration another one can be started to reach the desired shape of the product [106].

Chapter 5

Conclusions and Recommendations

Conclusions

Springback prediction and compensation are the major challenges in the modern die manufacturing industry. In spite of plenty of developments and a certain amount of progress in the field of simulation of sheet metal forming processes, the industrial needs for accurate numerical prediction of springback are not yet being met. The objective of this literature study is to identify the reasons of poor accuracy of prediction of springback phenomenon in sheet metal forming.

As was explained in chapter 1 springback is caused by the relief of the internal bending moments. This fact suggests that all the factors which govern the development of the internal stresses in the material during loading and unloading have an influence on springback. High accuracy of the stress state can only be obtained if an appropriate material model is used. It must be based on the initial yielding and hardening characteristics obtained from multiple tests. The material model should be able to describe the material behaviour when it undergoes an arbitrary loading path. In particular, the effects of strain path changes must be accounted for.

Initial value of Young's modulus is anisotropic. It depends on the material in plane direction and the amount of thickness reduction during rolling. In addition to it, the variation of the Young's modulus during the deformation process is another important reason of usual underestimation of springback. It was shown in several studies that elastic modulus of a material decreases by $10-20\%$ during the plastic deformation reaching the saturation value after 5-7% of plastic strain. The saturation value strongly depends on the loading path and the evolution of the material microstructure during forming.

Slight variations of a yield stress, R-values, hardening parameters and a sheet thickness - comparable with scatter of material properties due to production process - hardly influence the springback behaviour. This influence can become more significant for products with low level of plastic deformation.

It is clear that the abilities of analytical methods to predict the level of springback of complex products are limited and the use of finite element method is required. The accuracy

of finite element software has a significant influence on the change of shape during unloading. Large modelling and discretization errors, due to the chosen element types, the mesh sizes and the amount of integration points through the thickness, may cause a substantial deviation from the accurate solution, and therefore:

- for small values of the R/t ratio (the radius of the tool to the sheet thickness) the underlying assumptions of the shell elements theory are not applicable. For this situation the 3D solid elements are needed to describe the fully three dimensional stress state;
- for high accuracy of springback prediction up to 20 elements in the region of the tool radius are needed to discretize the blank. If used, adaptive mesh refinement procedures should be applied with caution;
- a large number of integration points through the thickness produces more accurate results.

The unloading scheme has an influence on springback prediction. The commonly used instantaneous unloading procedure is proved to produce inaccurate results. During unloading the existing contact forces can cause the additional change of shape of the formed product. Moreover, the instantaneous unloading method is not applicable for predicting springback of buckling dominated problems. The gradual unloading method, which takes into consideration the interaction between the tools and the blank during springback, should be used. Due to the fact that the unloading sequence has an influence on springback prediction it is suggested to apply the same retracting sequence of the tools in the simulation as during the experiments. Partial gradual unloading, followed by the instantaneous release, gives the same results as the complete gradual release. This method is very attractive from the economic point of view.

Stabilization techniques which can be internally used in a finite element software may have a significant influence on springback behaviour. Application of the numerical damping during the springback step must be minimised to avoid the unrealistic deterioration of product shape.

The parameters of contact description largely influence the accuracy of the obtained numerical solution. If the penalty method is used the value of the contact stiffness must be sufficiently high to accurately describe the geometry of tools. The chosen value of the coefficient of friction may have a large influence on the accuracy of springback prediction. Moreover, advanced models, capable of describing the variation of the friction coefficient during forming, should be used.

Recommendations

To test available advanced yield functions and material hardening models, an additional study should be performed. The major goal of the study should be to check the level of improvement of springback prediction accuracy. Additional targets of the study can be an investigation on the levels of deviation of material properties and sheet thicknesses and

an understanding the sensitivity of springback to variation of parameters of material yield function and hardening model.

Simple models, which can emulate the change of elastic constants of a material during the deformation, must be implemented and tested. The subject of Young's modulus anisotropy and its dependency on the plastic strain should be studied in greater detail. Particular attention must be given to dependency of the Young's modulus saturation value upon the loading path and the deformation-induced anisotropy. Based on the outcomes of this study the required updates of the models describing the variation of the Young's modulus should be made.

An additional study is required to specify the guidelines on the level of mesh fineness of blank and tools. The efficacy and feasibility of the mixed solid-shell elements approach should be investigated. The possibility of making the number of integration points or their position through the thickness variable - depending on the value of curvature or through thickness stress gradient - should be studied.

The major drawback of the gradual unloading method - poor convergence of the simulation and, therefore, increased computation time - should be addressed. A study should be performed on the possibility of improving the performance of contact algorithm during the sliding with low normal forces. Additionally, the feasibility of substituting the gradual unloading method with the two-steps release method should be investigated.

The expertise of the analyst will remain crucial in springback prediction. Therefore, the guidelines that will be developed in the course of this project should be used as a starting point in springback simulations.

Chapter 6

Future work

The decrease of Young's modulus during the deformation was reported for the situation when a sheet specimen was loaded in uniaxial tension or compression. However, the deep drawing process is characterised by a mixed type of loading conditions and the decrease of the elastic modulus can be less appreciable. Therefore, an additional research is necessary to study variation of the elastic modulus in realistic sheet metal forming conditions. The main subjects of the study are:

- investigation of the level of decrease of the elastic modulus in various loading conditions and its subsequent recovery;
- development of an appropriate model that describes the change of the Young's modulus during the deformation. The dependency of the saturation value of the elastic modulus on the deformation induced anisotropy and strain path changes must be accounted for in this model. The development of the model can be focused on accurately describing the extra inelastic strain that is recovered during unloading;
- investigation of performance of the developed model in realistic loading conditions.

Additionally, the elastic anisotropy must be addressed in this study. Based on the texture simulations of the rolling process of copper it was observed that the variation of the Young's modulus depending on the angle with the rolling direction can be significant. However, there is a need for some experimental proofs of the elastic anisotropy. Depending on its level the decision will be made about whether to incorporate this phenomenon into the Young's modulus variation model.

It is shown in the literature that some of the advanced yield functions are capable of more accurately describing the initial yielding of a material. Additionally, it is well known that the accuracy of the defined position of equi-biaxial, plane strain or plane stress points governs the accuracy of stress state after forming and consequently springback. To distinguish the maximum influence that the selected yield criterion may have on the accuracy of springback prediction a separate study is required. The Vegter, Barlat and Hill'48 yield functions are possible yield criteria that can be used in this study. The analysis must be

performed on various well-defined components. The sensitivity of springback to variation of parameters of advanced material models should be investigated additionally.

The quantitative sensitivity of springback to the chosen material hardening function must be investigated. The study can be started from evaluating the sensitivity of springback to the Bauschinger effect. Available hardening models that are able to describe 1 or 2 loading cycles will be used. The second part of the study can be dedicated to investigation of improving the accuracy of springback analysis by using the material hardening models which are capable of describing the effects of strain path changes. Based on the results of this study the new research directions for a separate project may be defined.

It is suggested in the literature that the solid elements are necessary for describing the fully three dimensional stress state which can occur when the r/t ratio is small. For this situation the underlying assumptions of the shell elements theory are not applicable. However, the use of only solid elements is not feasible, due to unrealistic requirements for CPU power. Alternatively, it is usually suggested to use the mixed solid-shell elements for blank discretization. Unfortunately, this approach has plenty of difficulties related to its implementation. The modification of shell elements - to make them capable of behaving accurately in the regions with fully three-dimensional stress state - can be another interesting approach. Therefore, an additional study is required to investigate the main causes of discrepancy of results for the situations with low r/t ratio. The study can be split into several tasks:

- evaluation of performance of solid and shell elements in the regions with low values of r/t ratio using a simple simulation set-up;
- understanding the main reasons of bad performance of shell elements and defining the possible modifications. These modifications can be related to incorporating the influence of localised high contact stresses in the regions with fully three dimensional stress state or to taking into account the non-linear distribution of internal variables through the thickness;
- validation of performance of modified elements with respect to the accuracy of springback prediction.

It is believed that more than seven integration points in the thickness direction and about 20 elements over the tool radius are necessary for an accurate springback analysis. The sensitivity of springback to the amount of integration points through the sheet thickness and element sizes must be investigated. The main goal of the study is to develop the guidelines defining the amount of integration points and the level of discretization of a curvature by elements to be able to perform the accurate springback analysis. The tasks are generally described below:

- performing the simulations of NUMISHEET 1993 benchmark problem - top-hat section - to define the amount of elements needed to discretize the blank and the tools;

- selection of an appropriate integration scheme and performing a number of simulations of a well-characterised problem to define a number of integration points through the thickness. It is believed that the amount of integration points should be sufficient enough to capture the elastic-plastic transition during forming;
- investigation of the possibility of making the number of integration points variable during the simulation depending on the curvature. It is suggested that for the regions with low curvature less integration points can be used compared to the regions with high curvature.

The influence of the contact forces during unloading on the level of springback should be studied separately on a well-characterised component. The maximum effect on the accuracy of springback analysis from taking into account the contact forces during unloading should be understood.

Acknowledgements

This project (MC1.02121) is funded by the Netherlands Institute for Metals Research. The scientific support of the project members and the financial support of the Netherlands Institute for Metals Research are greatly acknowledged.

Bibliography

[1] Avetisyan M. *Numerical Trimming Operation with Respect to Springback*. Netherlands Institute for Metals Research, 2004.

[2] Wagoner R.H. Fundamental aspects of springback in sheet metal forming. In Huh H. Yang D.-Y., Oh S.I. and Kim Y.H., editors, *NUMISHEET 2002, The Fifth International Conference and Workshop on Numerical Simulation of 3D Sheet Forming Processes.*, pages 13 – 24, Jeju Island, Korea, 2002.

[3] Wang C. An industrtial outlook for springback predictability, measurement reliability and compensation technology. In Huh H. Yang D.-Y., Oh S.I. and Kim Y.H., editors, *NUMISHEET 2002, The Fifth International Conference and Workshop on Numerical Simulation of 3D Sheet Forming Processes.*, pages 597–604, Jeju Island, Korea, 2002.

[4] Makinouchi A. Sheet metal forming simulation in industry. *Journal of Materials Processing Technology*, 60(1-4):19–26, 1996.

[5] Col A. Presentation of the "3ds" research project. In Huh H. Yang D.-Y., Oh S.I. and Kim Y.H., editors, *NUMISHEET 2002, The Fifth International Conference and Workshop on Numerical Simulation of 3D Sheet Forming Processes.*, pages 643 – 647, Jeju Island, Korea, 2002.

[6] Carden W.D., Geng L.M., Matlock D.K., and Wagoner R.H. Measurement of springback. *International Journal of Mechanical Sciences*, 44(1):79–101, 2002.

[7] Livatyali H. and Altan T. Prediction and elimination of springback in straight flanging using computer aided design methods: Part 1. experimental investigations. *Journal of Materials Processing Technology*, 117(1-2):262–268, 2001.

[8] Livatyali H., Kinzel C.L., and Altan T. Computer aided die design of straight flanging using approximate numerical analysis. *Journal of Materials Processing Technology*, 142(2):532–543, 2003.

[9] Livatyali H., Wu H.C., and Altan T. Prediction and elimination of springback in straight flanging using computer-aided design methods: Part 2: Fem predictions and tool design. *Journal of Materials Processing Technology*, 120(1-3):348–354, 2002.

[10] Leu D.-K. A simplified approach for evaluating bendability and springback in plastic bending of anisotropic sheet metals. *Journal of Materials Processing Technology*, 66(1-3):9–17, 1997.

[11] Asnafi N. Springback and fracture in v-die air bending of thick stainless steel sheets. *Materials & Design*, 21(3):217–236, 2000.

[12] Pourboghrat F. and Chu E. Springback in plane strain stretch/draw sheet forming. *International Journal of Mechanical Sciences*, 37(3):327, 1995.

[13] Zhang Z.T. and Hu S.J. Stress and residual stress distributions in plane strain bending. *International Journal of Mechanical Sciences*, 40(6):533–543, 1998.

[14] Asnafi N. On springback of double-curved autobody panels. *International Journal of Mechanical Sciences*, 43(1):5–37, 2001.

[15] Xue P., Yu T.X., and Chu E. An energy approach for predicting springback of metal sheets after double-curvature forming, part i: Axisymmetric stamping. *International Journal of Mechanical Sciences*, 43(8):1893–1914, 2001.

[16] Xue P., Yu T.X., and Chu E. An energy approach for predicting springback of metal sheets after double-curvature forming, part ii: Unequal double-curvature forming. *International Journal of Mechanical Sciences*, 43(8):1915–1924, 2001.

[17] Xue P., Yu T.X., and Chu E. Theoretical prediction of the springback of metal sheets after a double-curvature forming operation. *Journal of Materials Processing Technology*, 89-90:65–71, 1999.

[18] Pourboghrat F., Karabin M.E., Becker R.C., and Chung K. Hybrid membrane/shell method for calculating springback of anisotropic sheet metals undergoing axisymmetric loading. *International Journal of Plasticity*, 16(6):677–700, 2000.

[19] Akkerman R., van den Boogaard A.H., Brekelmans W.A.M., Geijselaers H.J.M., Huétink J., Meinders T., Peerlings R.H.J., de Rooij M.B., and Schipper D.J. *Mechanics of forming processes. Lecture notes.* Graduate school of Engineering Mechanics, 2003.

[20] Wang J.F., Wagoner R.H., Carden W.D., Matlock D.K., and Barlat F. Creep and anelasticity in the springback of aluminum. *International Journal of Plasticity*, 20(12):2209–2232, 2004.

[21] Li K.P., Carden W.P., and Wagoner R.H. Simulation of springback. *International Journal of Mechanical Sciences*, 44(1):103–122, 2002.

[22] Kuwabara T., Asano Y., Ikeda S., and Hayashi H. An evaluation method for springback characteristics of sheet metals based on a stretch bending test. In Kergen R., Kebler L., Langerak N., Lenze F.-J., Janssen E., and Steinbeck G., editors, *IDDRG 2004. Forming the Future. Global Trends in Sheet Metal Forming.*, pages 55 – 64, Sindelfingen, Germany, 2004.

[23] Meinders T., Konter A.W.A., Meijers S.E., Atzema E.H., and Kappert H. A sensitivity analysis on the springback behaviour of the unconstrained bending problem. *Journal of Materials Processing Technology*, submitted for publication.

[24] Chou I.N. and Hung C. Finite element analysis and optimization on springback reduction. *International Journal of Machine Tools & Manufacture*, 39(3):517–536, 1999.

[25] Han S.S. and Park K.C. An investigation of the factors influencing springback by empirical and simulative techniques. In *NUMISHEET'99. The 4th International Conference and Workshop on Numerical Simulation of 3D Sheet Forming Processes*, pages 53–58, Besancon, France, 1999.

[26] Tekiner Z. An experimental study on the examination of springback of sheet metals with several thicknesses and properties in bending dies. *Journal of Materials Processing Technology*, 145(1):109–117, 2004.

[27] Zhang L.C., Lu G., and Leong S.C. V-shaped sheet forming by deformable punches. *Journal of Materials Processing Technology*, 63(1-3):134–139, 1997.

[28] Liu G., Lin Z., Xu W., and Bao Y. Variable blankholder force in u-shaped part forming for eliminating springback error. *Journal of Materials Processing Technology*, 120(1-3):259–264, 2002.

[29] Xu W.L., Ma C.H., Li C.H., and Feng W.J. Sensitive factors in springback simulation for sheet metal forming. *Journal of Materials Processing Technology*, 151(1-3):217–222, 2004.

[30] E. Bayraktar and S. Altintas. Square cup deep drawing and 2d-draw bending analysis of hadfield steel. *Journal of Materials Processing Technology*, 60(1-4):183–190, 1996.

[31] Li K., Geng L., and Wagoner R.H. Simulation of springback: Choice of element. In M. Geiger, editor, *Advanced Technology of Plasticity 1999*, volume 3, pages 2091 – 2099, Nuremberg, Germany, 1999. Springer-Verlag.

[32] Geng L., Yao S., and Wagoner R.H. Anisotropic hardening equations derived from reverse-bend testing. *International Journal of Plasticity*, 18(5):743–767, 2002.

[33] Chun B. K., Jinn J. T., and Lee J. K. Modeling the bauschinger effect for sheet metals, part i: theory. *International Journal of Plasticity*, 18(5-6):571–595, 2002.

[34] Cleveland R. M. and Ghosh A. K. Inelastic effects on springback in metals. *International Journal of Plasticity*, 18(5-6):769–785, 2002.

[35] Yoshida F., Uemori T., and Fujiwara K. Elastic-plastic behavior of steel sheets under in-plane cyclic tension-compression at large strain. *International Journal of Plasticity*, 18(6):633–659, 2002.

[36] Zhao K.M. and Lee J.K. Finite element analysis of the three-point bending of sheet metals. *Journal of Materials Processing Technology*, 122(1):6–11, 2002.

[37] Yoshida F., Urabe M., and Toropov V.V. Identification of material parameters in constitutive model for sheet metals from cyclic bending tests. *International Journal of Mechanical Sciences*, 40(2-3):237–249, 1998.

[38] Gau J.-T. and Kinzel G. L. A new model for springback prediction in which the bauschinger effect is considered. *International Journal of Mechanical Sciences*, 43(8):1813–1832, 2001.

[39] Gau J.-T. and Kinzel G. L. An experimental investigation of the influence of the bauschinger effect on springback predictions. *Journal of Materials Processing Technology*, 108(3):369–375, 2001.

[40] Huétink J., Streppel A.H., and Vreede P.T. Development and experimental verification of constitutive equations for anisotropic sheet metal. In Owen D.R.J., Onate E., and Hinton E., editors, *Complas95*, volume 2, pages 2271–2282, 1995.

[41] Lems W. *The change of Young's modulus after deformation at low temperature and its recovery.* PhD thesis, Delft University of Technology, 1963.

[42] Morestin F. and Boivin M. On the necessity of taking into account the variation in the young modulus with plastic strain in elastic-plastic software. *Nuclear Engineering and Design*, 162(1):107–116, 1996.

[43] Iwata I. and Matsui M. Numerical prediction of spring-back behavior of a stamped metal sheet by considering material non-linearity during unloading. In Ken ichiro Mori, editor, *Numiform2001*, pages 693–698, Toyohashi, Japan, 2001.

[44] Thibaud S., Boudeau N., and Gelin J-C. On the influence of the young modulus evolution on the dynamic behaviour and springback of a sheet metal forming component. In Huh H. Yang D.-Y., Oh S.I. and Kim Y.H., editors, *NUMISHEET 2002, The Fifth International Conference and Workshop on Numerical Simulation of 3D Sheet Forming Processes.*, pages 149 – 153, Jeju Island, Korea, 2002.

[45] Yang M., Akiyama Y., and Sasaki T. Evaluation of change in material properties due to plastic deformation. *Journal of Materials Processing Technology*, 151(1-3):232–236, 2004.

[46] Li X., Yang Y., Wang Y., Bao J., and Li S. Effect of the material-hardening mode on the springback simulation accuracy of v-free bending. *Journal of Materials Processing Technology*, 123(2):209–211, 2002.

[47] de Vin L. J., Streppel A. H., Singh U. P., and Kals H. J. J. A process model for air bending. *Journal of Materials Processing Technology*, 57(1-2):48–54, 1996.

[48] Krasowsky A., Walde T., Schmitt W., Andrieux F., and Riedel H. Springback simulation in sheet metal forming using material formulation based on combined isotropic-kinematic hardening with elasto-plastic anisotropy. In Kergen R., Kebler L., Langerak N., Lenze F.-J., Janssen E., and Steinbeck G., editors, *IDDRG 2004. Forming the Future. Global trends in sheet metal forming.*, pages 104 – 113, Sindelfingen, Germany, 2004.

[49] Atzema E.H., Kappert H., Konter A.W.A., Meijers S.E., and Meinders T. *Sensitivity analysis component 2: Scaled down car roof.* Netherlands Institute for Metals Research, 2005.

[50] Luo and Ghosh A. K. Elastic and inelastic recovery after plastic deformation of dqsk steel sheet. *Journal of Engineering Materials and Technology, Transactions of the ASME*, 125(3):237–246, 2003.

[51] Barlat F., Banabic D., and Cazacu. Anisotropy in sheet metals. In Huh H. Yang D.-Y., Oh S.I. and Kim Y.H., editors, *NUMISHEET 2002, The Fifth International Conference and Workshop on Numerical Simulation of 3D Sheet Forming Processes.*, pages 515 – 524, Jeju Island, Korea, 2002.

[52] Pijlman H. *Sheet material characterisation by multi-axial experiments.* PhD thesis, University of Twente, 2001.

[53] Carleer B.D., Meinders T., Pijlman H.H., Huétink J., and Vegter H. A planar anisotropic yield function based on multi axial stress states in finite elements. In Owen D.R.J., Onate E., and Hinton E., editors, *Complas97*, pages 913–920, 1997.

[54] Aretz H. Applications of a new plane stress yield function to orthotropic steel and aluminium sheet metals. *Modelling and Simulation in Materials Science and Engineering*, 12(3):491–509, 2004.

[55] Yoon J.-W., Barlat F., Dick R. E., Chung K., and Kang T. J. Plane stress yield function for aluminum alloy sheets - part ii: Fe formulation and its implementation. *International Journal of Plasticity*, 20(3):495–522, 2004.

[56] Hiwatashi S., Van Bael A., Van Houtte P., and Teodosiu C. Modelling of plastic anisotropy based on texture and dislocation structure. *Computational Materials Science*, 9(1-2):274–284, 1997.

[57] Alves J.L., Oliveira M.C., and Menezes L.F. Springback evaluation with several phenomenological yield criteria. In *II International Materials Symposium.*, volume 455-456 of *Materials Science Forum*, pages 732–736, Caparica, Portugal, 2004.

[58] Lademo O.-G., Hopperstad O.S., and Langseth M. An evaluation of yield criteria and flow rules for aluminum alloys. *International Journal of Plasticity*, 15(2):191–208, 1999.

[59] Mattiasson K. and Sigvant M. Material characterization and modeling for industrial sheet forming simulations. In Ghosh S., Castro J.M., and Lee J.K., editors, *Numiform2004. Materials Processing and Design: Modeling, Simulation and Applications.*, pages 875 – 880, Columbus, Ohio, 2004.

[60] Berg H., Hora P., and Reissner J. Simulation of sheet metal forming processes using different anisotropic constitutive models. In Huétink J. and Baaijens F.P.T., editors, *NUMIFORM'98. Simulation of Material Processing: Theory, Methods and Applications.*, pages 775 – 780, Enschede, The Netherlands, 1998.

[61] van den Boogaard T. *Thermally enhanced forming of aluminium sheet*. PhD thesis, University of Twente, 2002.

[62] Huétink J. and Meinders T. *Forming technology. Plasticity and Creep. Lecture notes.* University of Twente, 2003.

[63] Yoshida F. and Uemori T. A model of large-strain cyclic plasticity and its application to springback simulation. *International Journal of Mechanical Sciences*, 45(10):1687–1702, 2003.

[64] Yoshida F. and Uemori T. A model of large-strain cyclic plasticity describing the bauschinger effect and workhardening stagnation. *International Journal of Plasticity*, 18(5):661–686, 2002.

[65] Chun B. K., Kim H. Y., Lee, and J. K. Modeling the bauschinger effect for sheet metals, part ii: applications. *International Journal of Plasticity*, 18(5-6):597–616, 2002.

[66] Wagoner R.H. and Geng L. Role of plastic anisotropy and its evolution on springback. *International Journal of Mechanical Sciences*, 44(1):123–148, 2002.

[67] Prager W. Recent developments in the mathematical theory of plasticity. *Journal of applied physics*, (20):235, 1949.

[68] Ziegler H. A modification of Prager's hardening rule. *Journal of applied mathematics*, 55:187–192, 1959.

[69] Mroz Z. On generalized kinematic hardening rule with memory of maximum prestress. *Journal of applied mechanics*, pages 241 – 259, 1981.

[70] Krieg R.D. A practical two surface plasticicty theory. *Journal of applied mechanics*, pages 641 – 646, 1975.

[71] Jiang Y. and Kurath P. Characteristics of the armstrong-frederick type plasticity models. *International Journal of Plasticity*, 12(3):387–415, 1996.

[72] Ristinmaa M. Cyclic plasticity model using one yield surface only. *International Journal of Plasticity*, 11(2):163–181, 1995.

[73] Chaboche J.L. Time-independent constitutive theories for cyclic plasticity. *International Journal of Plasticity*, 2(2):149 – 188, 1986.

[74] Li S., Hoferlin E., Van Bael A., Van Houtte P., and Teodosiu C. Finite element modeling of plastic anisotropy induced by texture and strain-path change. *International Journal of Plasticity*, 19(5):647, 2003.

[75] Viatkina E.M., Brekelmans W.A.M., and Geers M.G.D. Modelling of strain path change effects on the basis of dislocation structure evolution. In *NIMR Congress 2003 "Building Bridges in Metallurgy"*, page 79, Noordwijkerhout, 2003.

[76] Hu Y. Quasi static finite element algorithms for sheet metal stamping springback simulation. In Gelin J.C. and Picart P., editors, *NUMISHEET'99. The 4th International Conference and Workshop on Numerical Simulation of 3D Sheet Forming Processes.*, pages 71 – 76, Besancon, France, 1999.

[77] Karafillis A. P. and Boyce M. C. Tooling and binder design for sheet metal forming processes compensating springback error. *International Journal of Machine Tools & Manufacture*, 36(4):503–526, 1996.

[78] Papeleux L. and Ponthot J.-P. Finite element simulation of springback in sheet metal forming. *Journal of Materials Processing Technology*, 125-126:785–791, 2002.

[79] Joannic D. and Gelin J.C. Shape defects in sheet metal forming operations after springback. In Gelin J.C. and Picart P., editors, *NUMISHEET'99. The 4th International Conference and Workshop on Numerical Simulation of 3D Sheet Forming Processes.*, pages 29 – 34, Besancon, France, 1999.

[80] van den Boogaard A.H., Meinders T., and Huétink J. Efficient implicit finite element analysis of sheet forming processes. *International Journal for Numerical Methods in Engineering*, 56(8):1083–1107, 2003.

[81] Lee S. W. and Yang D. Y. An assessment of numerical parameters influencing springback in explicit finite element analysis of sheet metal forming process. *Journal of Materials Processing Technology*, 80-81:60–67, 1998.

[82] Narasimhan N. and Lovell M. Predicting springback in sheet metal forming: An explicit to implicit sequential solution procedure. *Finite Elements in Analysis and Design*, 33(1):29–42, 1999.

[83] Finn M. J., Galbraith P. C., Wu L., Hallquist J. O., Lum L., and Lin T. L. Use of a coupled explicit–implicit solver for calculating spring-back in automotive body panels. *Journal of Materials Processing Technology*, 50(1-4):395–409, 1995.

[84] Li G.Y., Tan M.J., and Liew K.M. Springback analysis for sheet forming processes by explicit finite element method in conjunction with the orthogonal regression analysis. *International Journal of Solids and Structures*, 36(30), 1999.

[85] Jung D.W. Static-explicit finite element method and its application to drawbead process with spring-back. *Journal of Materials Processing Technology*, 128(1-3):292–301, 2002.

[86] Yang D.Y., Jung D.W., Song I.S., Yoo D.J., and Lee J.H. Comparative investigation into implicit, explicit, and iterative implicit/explicit schemes for the simulation of sheet-metal forming processes. *Journal of Materials Processing Technology*, 50(1-4):39–53, 1995.

[87] Oliveira M.C., J.L. Alves, and L.F. Menezes. Springback evaluation using 3-d finite elements. In Huh H. Yang D.-Y., Oh S.I. and Kim Y.H., editors, *NUMISHEET 2002, The Fifth International Conference and Workshop on Numerical Simulation of 3D Sheet Forming Processes.*, pages 189 – 194, Jeju Island, Korea, 2002.

[88] Jung D.W. and Yang D.Y. Step-wise combined implicit-explicit finite-element simulation of autobody stamping processes. *Journal of Materials Processing Technology*, 83(1-3):245–260, 1998.

[89] Noels L., Stainier L., and Ponthot J. P. Combined implicit/explicit time-integration algorithms for the numerical simulation of sheet metal forming. *Journal of Computational and Applied Mathematics*, 168(1-2):331–339, 2004.

[90] Muthler A., Dster A., Volk W., Wagner M., and Rank E. High order finite elements applied to the computation of elastic spring back in sheet metal forming. In Ghosh S., Castro J.M., and Lee J.K., editors, *Numiform2004. Materials Processing and Design: Modeling, Simulation and Applications.*, pages 946 – 951, Columbus, Ohio, 2004.

[91] Alves J.L. and Menezes L.F. Application of tri-linear and tri-quadratic 3-d solid elements in sheet metal forming process simulations. In Ken ichiro Mori, editor, *Numiform2001*, pages 639 – 644, Toyohashi, Japan, 2001.

[92] Menezes L.F. and Teodosiu C. Three-dimensional numerical simulation of the deep-drawing process using solid finite elements. *Journal of Materials Processing Technology*, 97(1-3):100–106, 2000.

[93] Xia C. Z. A parametric study of springback behavior. In Ken ichiro Mori, editor, *Numiform2001*, pages 711–716, Toyohashi, Japan, 2001.

[94] Park D.-W. and Oh S.-I. A four-node shell element with enhanced bending performance for springback analysis. *Computer Methods in Applied Mechanics and Engineering*, 193(23-26):2105–2138, 2004.

[95] Xia Z.C., Tang S.C., and Carnes J.C. Accurate springback prediction with mixed solid/shell elements. In Huétink J. and Baaijens F.P.T., editors, *NUMIFORM'98. Simulation of Material Processing: Theory, Methods and Applications.*, pages 813 – 818, Enschede, The Netherlands, 1998.

[96] N. Montmayeur and C. Staub. Springback prediction with optris. In Gelin J.C. and Picart P., editors, *NUMISHEET'99. The 4th International Conference and Workshop on Numerical Simulation of 3D Sheet Forming Processes.*, pages 41 – 46, Besancon, France, 1999.

[97] Shim H. and Suh E. Contact treatment algorithm for the trimmed nurbs surface. *Journal of Materials Processing Technology*, 104(3):200–206, 2000.

[98] Santos A. and Makinouchi A. Contact strategies to deal with different tool descriptions in static explicit fem for 3-d sheet-metal forming simulation. *Journal of Materials Processing Technology*, 50(1-4):277–291, 1995.

[99] Atzema E.H. *Formability of sheet metal and sandwich laminates.* PhD thesis, University of Twente, 1994.

[100] Kloosterman G. *Contact methods in finite element simulations.* PhD thesis, University of Twente, 2002.

[101] Vreede P.T., Carleer B.D., Louwes M.F.M., and Huétink J. Finite-element simulation of sheet-forming processes with the help of contact elements on small-scale workstations. *Journal of Materials Processing Technology*, 50(1-4):264–276, 1995.

[102] Cao J. Consistent and minimal springback using a stepped binder force trajectory and neural network control. *Journal of Engineering Materials and Technology, Transactions of the ASME*, 122:113 – 118, 2000.

[103] Gunnarsson L. and Schedin E. Improving the properties of exterior body panels in automobiles using variable blank holder force. *Journal of Materials Processing Technology*, 114(2):168–173, 2001.

[104] Du C., Wu J., Militisky M., Principe J., Garnett M., and Zhang L. Springback control with variable binder force experiments and fea simulation. In Ghosh S., Castro J.M., and Lee J.K., editors, *Numiform2004. Materials Processing and Design: Modeling, Simulation and Applications.*, pages 970 – 976, Columbus, Ohio, 2004.

[105] Kutt L. M., Nardiello J. A., Ogilvie P. L., Pifko A. B., and Papazian J. M. Nonlinear finite element analysis of springback. *Communications in Numerical Methods in Engineering*, 15(1):33–42, 1999.

[106] Rietman A.D., Kose K., Ohnimus S., Petzoldt M., and Weiher J. Recent advances in industrial applied numerical aided springback compensation. In Kergen R., Kebler L., Langerak N., Lenze F.-J., Janssen E., and Steinbeck G., editors, *IDDRG 2004. Forming the Future. Global Trends in Sheet Metal Forming.*, pages 38 – 44, Sindelfingen, Germany, 2004.